

Revisiting the Matter Creation Process: Observational Constraints on Gravitationally Induced Dark Energy and the Hubble Tension

Tiziano Schiavone^{*}

*SISSA-International School for Advanced Studies, Via Bonomea 265, 34136 Trieste, Italy
INFN, Sezione di Trieste, Via Valerio 2, I-34127 Trieste, Italy and
Institute of Space Sciences (ICE,CSIC), C. Can Magrans s/n, 08193 Barcelona, Spain*

Mariaveronica De Angelis[†]

*Departamento de Física Teórica, Facultad de Ciencias Físicas,
Universidad Complutense de Madrid, 28040 Madrid, Spain*

Luis A. Escamilla[‡]

Department of Physics, Istanbul Technical University, Maslak 34469 Istanbul, Türkiye

Giovanni Montani[§]

*ENEA, Nuclear Department, C.R. Frascati, Via E. Fermi 45, 00044 Frascati, Italy and
Physics Department, Sapienza University of Rome, P.le A. Moro 5, 00185 Roma, Italy*

Eleonora Di Valentino[¶]

*School of Mathematical and Physical Sciences, University of Sheffield,
Hounsfeld Road, Sheffield, S3 7RH, South Yorkshire, United Kingdom*

(Dated: January 21, 2026)

The persistent Hubble tension and the lack of a fundamental explanation for dark energy motivate the exploration of alternative mechanisms capable of reproducing late-time cosmic acceleration. In this work, we revisit gravitationally induced particle creation as a phenomenological non-equilibrium process that can effectively mimic a dynamical dark-energy component. Within the thermodynamic framework of open systems, we model the production of an unspecified particle species with constant intrinsic equation-of-state parameter and consider four phenomenological parametrisations of the particle-creation rate. The modified continuity and Friedmann equations lead to an effective negative pressure and a redshift-dependent effective equation of state, which we constrain using Cosmic Chronometers, Pantheon+ supernovae, DESI DR2 BAO, a compressed CMB likelihood, and SH0ES data. Using the full dataset combination, we find that particle-creation models provide fits comparable to Λ CDM, yielding $H_0 \simeq 69.3 \text{ km s}^{-1} \text{ Mpc}^{-1}$ and present-day effective dark-energy equation-of-state values close to $w_{\text{DE}}^{\text{eff}}(0) \simeq -1$, with all models predicting an accelerating Universe ($q_0 \simeq -0.55$). When the Hubble tension is assessed using early- and late-time dataset splits, particle-creation scenarios reduce its statistical significance to the $\simeq 2.4\sigma$ - 3σ level, compared to the 4.3σ discrepancy obtained in Λ CDM. Although deviations from Λ CDM remain mild and Bayesian model comparison indicates no statistical preference between models, gravitationally induced particle creation emerges as a viable late-time extension of the standard cosmological model and provides a consistent phenomenological framework for exploring departures from Λ CDM.

I. INTRODUCTION

The standard cosmological model, the Λ CDM paradigm, provides an excellent description of a wide range of observational data, including measurements of the cosmic microwave background [1–6], large-scale structure [7–14], and the expansion history of the Universe [15–19]. Despite its remarkable empirical success,

the model relies on the presence of a cosmological constant (or dark energy) to explain the observed late-time acceleration of the Universe, whose fundamental physical origin remains theoretically unexplained [20]. This limitation has motivated the investigation of alternative mechanisms, among which gravitationally induced particle creation has emerged as a particularly appealing scenario.

Originally formulated within the framework of non-equilibrium thermodynamics and open-system cosmology [21, 22], particle creation models introduce a matter creation rate that effectively generates a negative pressure. This mechanism can naturally drive cosmic acceleration without the need for an explicit dark energy component. The underlying idea is that a time-dependent gravitational field, interacting with the quantum vacuum, may

^{*} tiziano.schiavone@sissa.it

[†] mdeangel@ucm.es

[‡] torresl@itu.edu.tr

[§] giovanni.montani@enea.it

[¶] e.divalentino@sheffield.ac.uk

lead to continuous particle production. Although these models were initially developed to describe the early Universe, particle creation may persist throughout cosmic history and play a role at late times.

While the microphysical nature of the created particles remains uncertain, most studies have focused on the production of cold dark matter [23–26]. This choice is motivated by several arguments: particle creation could offer an explanation for the origin of dark matter itself, naturally generate the negative pressure required for accelerated expansion, and potentially alleviate the coincidence problem [27] by treating dark matter and dark energy as different manifestations of a single unified component.

More recently, the particle creation framework has been extended beyond cold dark matter to include exotic fluids and generalized relativistic species. For instance, Costa Netto and Silva [28] performed a thermodynamic analysis of dark energy modeled as a relativistic fluid undergoing particle creation and annihilation. A more general multi-fluid extension was proposed by Trevisani and Lima [29], who studied gravitationally induced particle production in a decoupled cosmology involving baryons, photons, neutrinos, and dark matter. Additional developments include the gravitational production of a reduced relativistic gas [30] and connections with entropic cosmology [31], suggesting intriguing links between information-theoretic concepts and matter creation.

The versatility of the particle creation framework is further illustrated by its successful implementation within modified gravity theories. Matter creation naturally arises in scalar–tensor and $f(R, T)$ models [32], energy–momentum squared gravity [33, 34], and $f(R)$ theories [35], often leading to distinctive phenomenological signatures. Related scenarios have been explored in $f(R)$ models with entropic production [36], scalar–tensor theories with evolving vacuum energy [37], and effective fluid descriptions in non-Riemannian geometries [38]. These models are increasingly being tested against cosmological observations, particularly those probing the background expansion and the growth of large-scale structure [39, 40]. From a thermodynamic perspective, their internal consistency is supported by the validity of the generalized second law [41], while phenomenologically they share similarities with bulk viscous models [42], exotic fluids such as Chaplygin gases [43, 44], and unified dark energy scenarios that may exhibit phantom-like behavior.

Motivated by these developments, we extend the investigation of particle creation mechanisms in the context of late-time cosmology. In this work, we contribute to this growing line of research by generalising cosmological models based on particle creation. Rather than focusing on cold dark matter, we propose the gravitational production of an unknown particle species, characterised by an arbitrary equation-of-state parameter treated as a free variable. We assume negligible creation rates for radiation and cold dark matter (i.e., their particle numbers

remain conserved as the Universe expands), while the created species effectively behaves as a dark energy component. We then explore the implications of this mechanism for late-time cosmic acceleration and examine its potential role in addressing the Hubble tension, providing an alternative interpretation of the observed expansion history of the Universe.

The Hubble tension, referring to the discrepancy between local and early-Universe measurements of the Hubble constant H_0 , has been extensively documented in the literature [45–60]. More specifically, the Planck collaboration reports $H_0^P = (67.36 \pm 0.54) \text{ km s}^{-1} \text{ Mpc}^{-1}$ from cosmic microwave background radiation (CMB) data [2] (TT, TE, EE + lowE + lensing), while the SH0ES collaboration finds a significantly higher local value, $H_0^{\text{loc}} = (73.04 \pm 1.04) \text{ km s}^{-1} \text{ Mpc}^{-1}$, based on Cepheid-calibrated Type Ia supernovae (SNe Ia) [61], corresponding to a $\sim 5\sigma$ discrepancy. More recently, this tension has increased to the 7.1σ level when combining the latest CMB measurements from Planck+SPT+ACT [6] with the updated local measurement from the H0DN network [62], which provides a new consensus value for the distance-ladder determinations.

In response to the Hubble tension, a wide variety of models have been proposed, including those invoking modified gravity [63–75], self-interacting scalar fields [76], bulk viscosity [77, 78], and interactions within the dark sector [79–115]. Other studies have revisited the statistical assumptions and binning procedures used in cosmological data analyses, suggesting that methodological biases might contribute to the observed discrepancy [116–120]. Recent investigations have also pointed to a possible redshift evolution in the inferred values of H_0 , Ω_{m0} , or the absolute magnitude of Type Ia supernovae within standard Λ CDM fits across different redshift bins [64, 69, 74, 76, 121–137]. These trends have been interpreted as potential evidence for a local underdensity, departures from General Relativity, or the need for a dynamical dark energy component, *e.g.*, the $w_0 w_a$ CDM model according to the Chevallier-Polarski-Linder (CPL) parameterization [138, 139].

In this context, recent studies [78, 140, 141] have investigated matter creation as a viable mechanism to address the Hubble tension in connection with evolving dark energy models. These results further support the idea that gravitationally induced particle production may provide a unified, thermodynamically consistent framework capable of explaining both late-time acceleration and the observed tensions in cosmological data.

The paper is organized as follows. In Section II, we introduce the theoretical framework of gravitationally induced particle creation and derive the corresponding background equations. Section IV discusses the theoretical constraints on the model parameters, while Section V describes the observational datasets and statistical methodology employed. The main cosmological results are presented in Section VI, with particular emphasis on late-time acceleration, the effective dark energy behavior,

and the Hubble tension. Finally, Section VII summarizes our conclusions and outlines possible directions for future work.

II. PARTICLE CREATION IN COSMOLOGY

In this section, we develop the thermodynamic framework describing gravitationally induced particle creation, which provides the theoretical foundation for the cosmological models investigated in the following sections. The idea that a time-dependent gravitational field can lead to matter production can be phenomenologically formulated within the non-equilibrium thermodynamic approach developed in Refs. [22, 24–26].

A key assumption of this framework is the existence of a particle species whose total number N within a physical volume V is not conserved. Consequently, the standard particle number conservation equation is modified to

$$\nabla_\mu N^\mu = n\Gamma, \quad (1)$$

where ∇_μ denotes the covariant derivative compatible with the underlying spacetime metric (to be specified later), the coordinate indices are $\mu = \{0, \dots, 3\}$, $N^\mu = nu^\mu$ is the particle flux vector, $n = N/V$ is the number density, u^μ is the particle four-velocity, and Γ represents the particle creation (or annihilation) rate. The source term $n\Gamma$ therefore quantifies the rate of change of the particle number per unit volume due to non-conservation. Using the definition of N^μ , Eq. (1) can equivalently be written as

$$\partial_\mu n u^\mu + \Theta n = n\Gamma, \quad (2)$$

where $\Theta \equiv \nabla_\mu u^\mu$ is the expansion scalar. Eq. (2) follows directly from taking the covariant divergence of the particle flux and is commonly employed in the study of relativistic fluids (see, e.g. [24]). When $\Gamma = 0$, particle number conservation is restored, recovering the standard scenario.

Since the functional form of Γ is not known *a priori*, different particle creation models can be explored and subsequently constrained by observational data. When particle number is not conserved, the first and second laws of thermodynamics for open systems lead to the generalized relation

$$dU = -p dV + T dS + \mu dN, \quad (3)$$

where U is the internal energy, p is the pressure, T is the temperature, S is the entropy, and μ is the chemical potential. Writing $U = \rho V$ and $S = \sigma N$, with ρ the energy density and σ the specific entropy per particle, the chemical potential follows from the Gibbs relation [142], yielding $\mu = (\rho + p)V/N - T\sigma$. Substituting this expression into Eq. (3) gives

$$d\rho = -(\rho + p) \left(1 - \frac{d \ln N}{d \ln V} \right) \frac{dV}{V} + T \frac{N}{V} d\sigma. \quad (4)$$

In contrast to a isentropic system, we only require the specific entropy to be conserved, *i.e.*, $d\sigma = 0$. Since $\sigma = S/N$, this implies $S \propto N$, indicating that particle creation increases the total entropy.

We now consider a fiducial volume in a spatially flat, homogeneous, and isotropic Universe, consistent with *Planck* satellite observations [2]. The spacetime geometry on large cosmological scales is described by the Friedmann-Lemaitre-Robertson-Walker (FLRW) line element [143]:

$$ds^2 = dt^2 - a^2(t) [dr^2 + r^2 (d\theta^2 + \sin^2 \theta d\phi^2)], \quad (5)$$

where t is the comoving time, $\{r, \theta, \phi\}$ are spherical coordinates, and $a(t)$ is the scale factor. We adopt natural units ($c = 1$). The dynamics of cosmic expansion are governed by the Friedmann equation,

$$H^2 \equiv \left(\frac{\dot{a}}{a} \right)^2 = \frac{\chi}{3} \rho, \quad (6)$$

where $\chi = 8\pi G$ is the Einstein constant, $H = H(t)$ is the Hubble parameter, and an overdot denotes differentiation with respect to time. The total energy density $\rho = \rho_m + \rho_r + \rho_E$ includes matter (*e.g.*, baryons and dark matter), radiation, and an extra component E associated with particle creation. We assume that only this additional component exhibits a non-vanishing particle creation rate (*i.e.*, $\Gamma_E \neq 0$), while $\Gamma_m = \Gamma_r = 0$. For simplicity, we drop the subscript E and denote its creation rate by Γ . We exclude a cosmological constant, as our goal is to attribute the observed cosmic acceleration to the effects of particle production.

In the FLRW background, Eq. (2) for the extra species becomes

$$\dot{n}_E + 3Hn_E \left(1 - \frac{\Gamma}{3H} \right) = 0, \quad (7)$$

where, in the comoving gauge, $u_E^\mu = \delta_t^\mu = (1, 0, 0, 0)$ and the scalar expansion is $\Theta = 3H$. If $\Gamma = 0$ or $\Gamma \ll 3H$, particle creation is negligible and the standard conservation law is recovered. For $\Gamma > 0$ ($\Gamma < 0$), particles are produced (annihilated).

Assuming that the specific entropy per particle remains constant within a fiducial volume in a homogeneous and isotropic Universe, Eq. (4) reduces to

$$\dot{\rho}_E = -(\rho_E + p_E) \left(1 - \frac{d \ln N_E}{d \ln V} \right) \frac{d \ln V}{dt}, \quad (8)$$

where $V = a^3 V_0$ in an expanding Universe, with V_0 a constant comoving volume. This leads to the generalised continuity equation for the extra component,

$$\dot{\rho}_E + 3H(\rho_E + p_E) = \Gamma(\rho_E + p_E), \quad (9)$$

where the particle creation rate is defined as

$$\Gamma \equiv \frac{\dot{N}_E}{N_E}. \quad (10)$$

The case $\Gamma = 0$ recovers the standard conservation equation for the extra component. Meanwhile, the matter and radiation components are assumed to be conserved separately, following the usual continuity equations:

$$\dot{\rho}_m + 3H(\rho_m + p_m) = 0, \quad \dot{\rho}_r + 3H(\rho_r + p_r) = 0. \quad (11)$$

To study late-time cosmic acceleration, we begin by differentiating Eq. (6) with respect to time. This yields the modified Raychaudhuri equation,

$$\dot{H} = -\frac{\chi}{2}(\rho + p) + \frac{\chi\Gamma}{6H}(\rho_E + p_E). \quad (12)$$

Using $\dot{H} = \ddot{a}/a - H^2$, we derive the cosmic acceleration equation including the effects of particle creation,

$$\frac{\ddot{a}}{a} = -\frac{\chi}{6}(\rho_m + 2\rho_r) - \frac{\chi\rho_E}{6} \left[(1 + 3w_E) - \frac{\Gamma}{H}(1 + w_E) \right], \quad (13)$$

where we assume a barotropic equation of state $p_i = w_i\rho_i$ for each component, with $w_m = 0$ for pressureless matter, $w_r = 1/3$ for radiation, and w_E treated as a constant free parameter for the extra species.

The second term on the right-hand side of Eq. (13) represents the contribution of the extra component and particle production. This term can drive acceleration (i.e., dark-energy-like behavior) even in the absence of exotic fluids with intrinsic negative pressure. Assuming $\Gamma, H, \rho_i > 0$, the condition for present-day acceleration is

$$w_E \left(3 - \frac{\Gamma_0}{H_0} \right) < \frac{\Gamma_0}{H_0} - 1, \quad (14)$$

where the subscript “0” denotes present-day values. The direction of the inequality depends on the sign of the factor $\left(3 - \frac{\Gamma_0}{H_0} \right)$, which is not known *a priori*. If $\Gamma = 0$, the standard condition for dark energy, $w_E < -1/3$, is recovered.

An alternative way to describe the non-equilibrium thermodynamic effects of particle creation is to introduce an effective pressure term, denoted by Π , into the energy-momentum tensor of the extra fluid. The modified tensor takes the form

$$T_{\mu\nu}^{(E)} = (\rho_E + p_E + \Pi) u_\mu^E u_\nu^E + (p_E + \Pi) g_{\mu\nu}. \quad (15)$$

The non-equilibrium pressure is related to the particle creation rate by

$$\Pi = -\frac{\Gamma}{3H}(\rho_E + p_E). \quad (16)$$

It can be shown that both the continuity equation (9) and the cosmic acceleration equation (13) can be equivalently derived from the condition $\nabla_\nu T_{(E)}^{\mu\nu} = 0$. Thus, particle creation can effectively generate a negative pressure, thereby contributing to the accelerated expansion of the Universe.

PC Models				
Model	Γ : PC rate	# extra params	$g(z)$	Λ CDM limit
PC1	$3\beta H_0 \left(\frac{H}{H_0} \right)^\alpha$	3: α, β, w_E	N	$\beta = 0$
PC2	$3\mu H$	1: ξ	A	$\mu = 0 (\xi = 0)$
PC3	$3\gamma H_0$	2: γ, w_E	N	$\gamma = 0$
PC4	$3\gamma H_0 + 3\mu H$	3: γ, μ, w_E	N	$\gamma = \mu = 0$

TABLE I. The functional form of the particle-creation rates and the number of additional free parameters entering the dimensionless Hubble function $E(z)$ for each PC model are listed in the second and third columns, respectively. Note that, for the PC2 model, the only extra parameter affecting the cosmological dynamics is $\xi = 3(1 + w_E)(1 - \mu)$. The last column indicates whether the continuity equation for the dimensionless energy density $g(z)$ admits an analytical solution (A) or requires a numerical one (N). Moreover, in the Λ CDM limit, $w_E = -1$ for all models.

To conclude this section, if the extra component is interpreted as cold dark matter and only one species is considered while neglecting relativistic particles at late times, our results reduce to those obtained in [23–26] (with “E” corresponding to “m” and $w_m = 0$). A similar treatment applies to the case of light relativistic particles, by identifying “E” with “r” and setting $w_r = 1/3$. More generally, we consider the gravitational production of particles characterized by an unspecified equation-of-state parameter w_E , which may effectively mimic dark energy in the late Universe. The strength of this approach lies in its agnosticism regarding the nature of the created particles, leaving w_E as a free parameter to be constrained by observations. In Section VI, we derive observational constraints on w_E and on the associated cosmological parameters for different particle creation models.

III. PHENOMENOLOGY OF THE PARTICLE CREATION PROCESS WITH DIFFERENT PARTICLE PRODUCTION RATES

A natural phenomenological assumption is to relate the particle creation process to the expansion rate of the Universe [25, 26]. In this section, we investigate different scenarios of gravitationally induced particle production, each characterised by a specific parametrisation of the particle creation rate Γ . To consider only slight deviations from Λ CDM, we assume that the particle-creation process operates exclusively in the late Universe ($z \leq 3$), while for higher redshifts the standard Λ CDM behaviour is recovered. Our goal is to assess whether such particle creation (PC) models can successfully account for the observed late-time cosmic acceleration and to examine their implications for the Hubble tension.

To ensure consistency with late-time cosmic evolution, we interpret the particle creation process as an evolving dark energy component and require that its present-day

energy density, ρ_{E0} , reproduces the vacuum energy density ρ_Λ in a flat Λ CDM model. This leads to a generalized Hubble parameter of the form $H(z) = H_0 E(z)$, where the dimensionless Hubble function is given by

$$E(z) = \sqrt{\Omega_{m0}(1+z)^3 + \Omega_{r0}(1+z)^4 + \Omega_{E0} g(z)}. \quad (17)$$

The redshift variable is defined as $z(t) = a_0/a(t) - 1$, with $a_0 = 1$ denoting the present-day value of the scale factor. The cosmological density parameters today are defined as $\Omega_{i0} = \rho_{i0}/\rho_{c0}$, where i corresponds to matter, radiation, or the extra component, and $\rho_{c0} = 3H_0^2/\chi$ is the present critical energy density. We express the energy density of the extra component as $\rho_E(z) = \rho_{E0} g(z)$, where $g(0) = 1$ by construction. The function $g(z)$ is determined by the continuity equation, which depends on the specific choice of Γ , and can be obtained either analytically or numerically. Evaluating Eq. (17) at $z = 0$ recovers the standard normalization condition $\Omega_{m0} + \Omega_{r0} + \Omega_{E0} = 1$. Within this framework, the extra component behaves as a dynamical dark energy candidate.

The continuity equation (see Eq. (9)) can be rewritten in terms of the redshift as

$$\rho'_E(z) = \frac{3(1+w_E)}{1+z} \left(1 - \frac{\Gamma}{3H}\right) \rho_E(z), \quad (18)$$

or equivalently, using the relations $H(z) = H_0 E(z)$ and $\rho_E(z) = \rho_{E0} g(z)$,

$$g'(z) = \frac{3(1+w_E)}{1+z} \left(1 - \frac{\Gamma}{3H_0 E(z)}\right) g(z), \quad (19)$$

where the prime denotes differentiation with respect to redshift. The chain rule $(\dots)' = -(1+z)H(\dots)'$, obtained from the definitions of redshift and the Hubble parameter, is used to express time derivatives in terms of redshift derivatives.

Eqs (17) and (19) together form a coupled system for the two unknown functions $E(z)$ and $g(z)$. Once a specific form of the particle creation rate Γ is specified and the initial condition $g(0) = 1$ is imposed, this system can be solved to determine the cosmological evolution of the model.

The four PC models considered in this work, together with their particle-creation rates and main features, are summarised in Table I and described in detail below.

A. PC1 model

We begin by considering the following ansatz for the PC rate, as proposed in [23, 25, 26]

$$\Gamma = 3\beta H_0 \left(\frac{H}{H_0}\right)^\alpha, \quad (20)$$

where α and β are dimensionless constants. This choice describes a dynamical and continuous creation process,

in which the particle production rate evolves with the expansion rate of the Universe. Equivalently, the number of created particles increases with cosmic time as the Universe expands.

Substituting Eq. (20) into Eq. (19) yields

$$g'(z) = 3 \frac{1+w_E}{1+z} [1 - \beta E(z)^{\alpha-1}] g(z), \quad (21)$$

where $E(z)$ is defined in Eq. (17). This model is characterised by three free parameters, α , β , and w_E , and the function $g(z)$ is obtained numerically from the initial condition $g(0) = 1$. The Λ CDM limit is recovered when $\beta \rightarrow 0$ and $w_E \rightarrow -1$ for finite values of α .

B. PC2 model

We now consider an alternative parametrisation of the particle creation rate

$$\Gamma = 3\mu H, \quad (22)$$

in which it scales linearly with the expansion rate of the Universe. For this choice, the continuity equation admits an exact analytical solution:

$$g(z) = (1+z)^\xi, \quad (23)$$

where $\xi = 3(1+w_E)(1-\mu)$. The corresponding Hubble function is

$$E(z) = \sqrt{\Omega_{m0}(1+z)^3 + \Omega_{r0}(1+z)^4 + \Omega_{E0}(1+z)^\xi}. \quad (24)$$

This formulation is equivalent to a w CDM scenario with a constant effective equation-of-state parameter for dark energy,

$$w_{\text{DE}}^{\text{eff}} = -1 + \frac{\xi}{3}. \quad (25)$$

Moreover, the PC1 model reduces to this PC2 case when $\alpha = 1$ and $\beta = \mu$. The Λ CDM limit is recovered when $\mu \rightarrow 0$ and $w_E \rightarrow -1$, or equivalently $\xi \rightarrow 0$.

C. PC3 model

We now consider the case of a constant particle creation rate,

$$\Gamma = 3\gamma H_0. \quad (26)$$

In this scenario, the continuity equation becomes

$$g'(z) = 3 \frac{1+w_E}{1+z} \left(1 - \frac{\gamma}{E(z)}\right) g(z). \quad (27)$$

This model is characterised by two free parameters, γ and w_E . As in the PC1 setup, the function $g(z)$ is obtained numerically from the initial condition $g(0) = 1$, in combination with Eq. (17). Note that the PC1 model reduces to PC3 when $\alpha = 0$ and $\beta = \gamma$. Trivially, the Λ CDM limit is achieved when $\gamma \rightarrow 0$ and $w_E \rightarrow -1$.

D. PC4 model

Finally, we examine a mixed ansatz that combines both constant and time-dependent contributions

$$\Gamma = 3\gamma H_0 + 3\mu H. \quad (28)$$

With this choice, the continuity equation becomes

$$g'(z) = 3 \frac{1+w_E}{1+z} \left(1 - \mu - \frac{\gamma}{E(z)} \right) g(z). \quad (29)$$

This PC4 model involves three free parameters, γ , μ , and w_E . The function $g(z)$ is obtained numerically from the initial condition $g(0) = 1$, together with Eq. (17). The Λ CDM limit is recovered when $\gamma \rightarrow 0$, $\mu \rightarrow 0$, and $w_E \rightarrow -1$.

IV. THEORETICAL CONSTRAINTS FOR COSMIC ACCELERATION

In this section, we examine the cosmological implications of particle-creation mechanisms and compare them with the standard cosmological-constant paradigm. Specifically, we analyse the deceleration parameter and derive the effective dark-energy equation of state.

A. Cosmic acceleration

The reduced Hubble function $E(z)$ given in Eq. (17) should closely reproduce the expansion history of the

Λ CDM model. In particular, the dynamics induced by the four PC models discussed above must be able to explain the current accelerated expansion by satisfying the condition in Eq. (14). For each model, this requirement translates into the following constraints:

$$\text{PC1: } w_E (1 - \beta) < \beta - \frac{1}{3}, \quad (30)$$

$$\text{PC2: } w_E (1 - \mu) < \mu - \frac{1}{3}, \quad (31)$$

$$\text{PC3: } w_E (1 - \gamma) < \gamma - \frac{1}{3}, \quad (32)$$

$$\text{PC4: } w_E (1 - \gamma - \mu) < \gamma + \mu - \frac{1}{3}. \quad (33)$$

To study the transition from a decelerated to an accelerated expansion of the Universe, we use the general definition of the deceleration parameter

$$q(z) = -\frac{\ddot{a}}{aH^2} = -\left(1 + \frac{\dot{H}}{H^2}\right) = -1 + \frac{1}{2} \left[\frac{1+z}{E^2(z)} \frac{d}{dz} (E^2(z)) \right]. \quad (34)$$

Assuming an extra component induced by the gravitational field, with the Hubble function given in Eq. (17), the deceleration parameter becomes

$$q(z) = -1 + \frac{3}{2} \left[\frac{\Omega_{m0} (1+z)^3 + \frac{4}{3} \Omega_{r0} (1+z)^4 + \Omega_{E0} g(z) (1+w_E)}{\Omega_{m0} (1+z)^3 + \Omega_{r0} (1+z)^4 + \Omega_{E0} g(z)} \right] - \frac{\Gamma}{2H} \frac{\Omega_{E0} g(z) (1+w_E)}{\Omega_{m0} (1+z)^3 + \Omega_{r0} (1+z)^4 + \Omega_{E0} g(z)}. \quad (35)$$

By considering the Γ -rates of the PC models, we can rewrite the last term of Eq. (35) as:

$$\text{PC1: } -\frac{3\beta}{2} \frac{\Omega_{E0} g(z) (1+w_E)}{[E(z)]^{3-\alpha}}, \quad (36)$$

$$\text{PC2: } -\frac{3\mu}{2} \frac{\Omega_{E0} g(z) (1+w_E)}{E^2(z)}, \quad (37)$$

$$\text{PC3: } -\frac{3\gamma}{2} \frac{\Omega_{E0} g(z) (1+w_E)}{E^3(z)}, \quad (38)$$

$$\text{PC4: } -\frac{3}{2} \left(\frac{\gamma}{E(z)} + \mu \right) \frac{\Omega_{E0} g(z) (1+w_E)}{E^2(z)}. \quad (39)$$

The present-day value ($z = 0$) of the deceleration parameter is given by:

$$q_0 = -\frac{\ddot{a}}{aH^2} \Big|_{t=t_0} = -\left(1 + \frac{\dot{H}}{H^2}\right) \Big|_{t=t_0} = -1 + \frac{1}{2} \frac{dE^2}{dz} \Big|_{z=0}$$

In the Λ CDM model the deceleration parameter is given by $q_0^{\Lambda\text{CDM}} = -1 + \frac{3}{2} \Omega_{m0} + 2\Omega_{r0}$. In the PC framework, deviations from this baseline arise due to the presence of the additional component and the specific form of the particle-creation rate. Specifically, for each PC model, the expression for q_0 becomes:

$$\text{PC1: } q_0 = q_0^{\Lambda\text{CDM}} + \frac{3}{2} \Omega_{E0} (1+w_E) (1-\beta), \quad (41)$$

$$\text{PC2: } q_0 = q_0^{\Lambda\text{CDM}} + \frac{1}{2} \Omega_{E0} \xi, \quad (42)$$

$$\text{PC3: } q_0 = q_0^{\Lambda\text{CDM}} + \frac{3}{2} \Omega_{E0} (1+w_E) (1-\gamma), \quad (43)$$

$$\text{PC4: } q_0 = q_0^{\Lambda\text{CDM}} + \frac{3}{2} \Omega_{E0} (1 + w_E) (1 - \gamma - \mu). \quad (44)$$

B. Effective equation-of-state parameter for dark energy

The particle-creation process can be reformulated in terms of an effective dark-energy equation of state $w_{\text{DE}}^{\text{eff}}(z)$. Indeed, the modified Friedmann equations take the form

$$H^2 = \frac{\chi}{3} (\rho_m + \rho_r + \rho_{\text{DE}}^{\text{eff}}), \quad (45)$$

$$\frac{\ddot{a}}{a} = -\frac{\chi}{6} (\rho_m + 2\rho_r) - \frac{\chi \rho_{\text{DE}}^{\text{eff}}}{6} [1 + 3w_{\text{DE}}^{\text{eff}}(z)], \quad (46)$$

where the effective dark-energy density evolves as

$$\rho_{\text{DE}}^{\text{eff}}(z) = \rho_{\text{DE}0}^{\text{eff}} \exp \left[3 \int_0^z \frac{ds}{1+s} (1 + w_{\text{DE}}^{\text{eff}}(s)) \right], \quad (47)$$

where $\rho_{\text{DE}0}^{\text{eff}}$ denotes its present-day value.

Therefore, by comparing Eq. (6) with Eq. (45), and Eq. (13) with Eq. (46), one can readily express the effective equation-of-state parameter for dark energy as

$$w_{\text{DE}}^{\text{eff}}(z) = w_E - \frac{\Gamma}{3H} (1 + w_E). \quad (48)$$

Taking the logarithm of Eq. (48), differentiating with respect to redshift, and using the relation $\rho_{\text{DE}}^{\text{eff}}(z) = \rho_E(z) = \rho_{E0}g(z)$, we obtain an alternative expression for the effective equation of state:

$$w_{\text{DE}}^{\text{eff}}(z) = -1 + \frac{1+z}{3} \frac{g'(z)}{g(z)}, \quad (49)$$

which is particularly convenient when the functional form of $g(z)$ is known. For clarity, note that w_E is constant and characterizes the intrinsic equation of state of the created component, whereas $w_{\text{DE}}^{\text{eff}}(z)$ is redshift-dependent and effectively incorporates the impact of gravitationally induced particle production through the rate Γ .

Using Eq. (48), we can write the effective equation-of-state parameter for each PC model introduced in Sect. III:

$$\text{PC1: } w_{\text{DE}}^{\text{eff}}(z) = w_E - \beta [E(z)]^{\alpha-1} (1 + w_E), \quad (50)$$

$$\text{PC2: } w_{\text{DE}}^{\text{eff}}(z) = -1 + \frac{\xi}{3}, \quad (51)$$

$$\text{PC3: } w_{\text{DE}}^{\text{eff}}(z) = w_E - \frac{\gamma}{E(z)} (1 + w_E), \quad (52)$$

$$\text{PC4: } w_{\text{DE}}^{\text{eff}}(z) = w_E - \left[\frac{\gamma}{E(z)} + \mu \right] (1 + w_E), \quad (53)$$

It is important to note that $w_{\text{DE}}^{\text{eff}}(0) < -1/3$ is required to consistently account for the current cosmic acceleration.

V. DATASETS AND METHODOLOGY

In this work we make use of `SimpleMC` [144] as the sampling code. We employ Nested Sampling [145] as implemented in the `dynesty` Python library [146], which also provides the Bayesian Evidence needed to compare the PC models against the ΛCDM and $w_0w_a\text{CDM}$ baselines. For most analyses we used 1024 live points and an accuracy of 0.01 (which serves as the convergence criterion for nested sampling), ensuring good precision in the estimation of the evidence and posterior distributions. For the joint analysis `CC+SN+SHOES+BAO+CMB`, we instead adopted 500 live points for each model, which was sufficient to achieve numerical convergence while significantly reducing the computational cost.

Our particle-creation (PC) models primarily affect late-time cosmology, in particular the background expansion history. In our setup, the particle-creation mechanism is assumed to operate only in the redshift range $0 < z < 3$, as specified in Sect. III, and standard ΛCDM behaviour is recovered at higher redshift. For this reason, we make use of background-only datasets that predominantly probe the low-redshift Universe ($z \lesssim 2$).

The datasets used are as follows: a catalogue of 15 Cosmic Chronometers, including their covariance matrix [147] (hereafter `CC`); the PantheonPlus sample of Type Ia Supernovae (SNe Ia) [15, 16], consisting of 1701 light curves from 1550 unique SNe Ia used to measure the distance modulus (referred to as `SN`); the latest DESI DR2 Baryon Acoustic Oscillation measurements [12, 148, 149], hereafter `BAO`; the SHOES calibration for the PantheonPlus catalogue [61], denoted `SHOES`; and a compressed (also referred to as *geometrical*) CMB likelihood, where the CMB is treated as a BAO measurement at $z \approx 1100$ using the Planck 2018 data release (for a discussion on how to adopt this approach, please refer to [150]), which will be referred to as `CMB`. For the PantheonPlus sample, we consider 1590 data points, corresponding to the effective number of independent distance-modulus measurements entering the likelihood, after accounting for the combination of multiple light curves and the impact of peculiar velocities.

As the datasets are independent from each other, when combining them for the parameter inference procedure we can obtain the joint χ^2 by simply adding the individual ones. As an example, for the case where the combination `BAO+CMB` is used, we would have:

$$\chi_{\text{total}}^2 = \chi_{\text{BAO}}^2 + \chi_{\text{CMB}}^2. \quad (54)$$

We then compute the χ^2 contribution from each dataset separately (`CC`, `SN`, `SHOES`, `BAO`, and `CMB`) in order to monitor the behaviour of the fits and to identify possible tensions within specific probes. However, for clarity and consistency in the presentation of results, we report only the total χ^2 for each model and dataset combination.

To investigate the Hubble tension within the PC framework, we analyse two separate combinations of these

datasets: the late-time set **CC+SN+SHOES** and the high-redshift set **BAO+CMB**. We then combine all probes into **CC+SN+SHOES+BAO+CMB** to maximise constraining power. Results for all three cases will be presented in the following section.

The priors for all parameters used in the analysis are chosen to be flat (agnostic) and can be found in Table II. These were chosen following a preliminary exploration of the PC models, aimed at evaluating the impact of different parameter values on the Hubble function (see the Appendix). For illustration, Figs. 7 and 8 show this procedure for the PC1 model. A similar analysis was carried out for each PC model.

Likewise, Fig. 9 show the dependence of the effective dark-energy equation of state on the model parameters within PC1, forming part of the prior-selection process. For reference, we also use the flat (zero-curvature) Λ CDM model; Fig. 1 displays the marginalised posteriors for the background parameters $h \equiv \frac{H_0}{100 \text{ km s}^{-1} \text{ Mpc}^{-1}}$ and Ω_{m0} obtained using the combined **CC+BAO+SN+SHOES+CMB** dataset. We also include the $w_0 w_a$ CDM model for comparison, as noted above.

Although the contribution of radiation (Ω_{r0}) to the normalised Friedmann equation is negligible at low redshift, it is nevertheless included in our analysis for consistency. Since we are interested in quantifying slight deviations from Λ CDM induced by the particle-creation mechanism, it is important to retain all standard cosmological components (including radiation) and isolate the impact of the non-standard contribution associated with particle creation. This ensures that any departure from the standard expansion history can be robustly attributed to the particle-creation sector rather than to an incomplete background modeling. To this end, we fix the CMB temperature and neutrino contributions and write the present-day radiation density parameter as

$$\Omega_{r0} = \Omega_{\gamma0} \left[1 + \frac{7}{8} \left(\frac{4}{11} \right)^{4/3} N_{\text{eff}} \right], \quad (55)$$

with the photon density parameter given by

$$\Omega_{\gamma0} = \frac{8\pi^5}{15} \frac{(K_B T_\gamma)^4}{h_P^3 c^5} \frac{8\pi G}{3H_0^2}, \quad (56)$$

where $N_{\text{eff}} = 3.046$ is the effective number of relativistic species, $T_\gamma = 2.7255$ K is the CMB temperature, K_B is the Boltzmann constant, h_P the Planck constant, c the speed of light, and $H_0 = 100 \text{ km s}^{-1} \text{ Mpc}^{-1}$. Using numerical values, we obtain

$$\Omega_{r0} = 4.183 \times 10^{-5} h^{-2}. \quad (57)$$

Thus, once the posterior distribution of h is known, Ω_{r0} may be treated as a derived parameter.

Finally, we perform a model comparison making use of the Bayesian Evidence. Following the definition of Bayes' theorem,

$$P(u|D, M) = \frac{L(D|u, M)P(u|M)}{E(D|M)}, \quad (58)$$

where u is the vector of free parameters to estimate, M is the model (also referred to as the *hypothesis*), D is the data, $P(u|D, M)$ is the posterior probability distribution, $L(D|u, M)$ is the *likelihood*, $P(u|M)$ is the prior distribution, and $E(D|M)$ is commonly referred to as the *Bayesian evidence*. During a parameter inference procedure, one uses a sampler code to find the posterior distribution of a model's parameters using data. This posterior distribution is obtained by sampling values of the parameters that maximize the likelihood. By relating the χ^2 , whose value decreases as the fit to the data improves, to the likelihood as

$$L \propto e^{-\frac{\chi^2}{2}}, \quad (59)$$

we can begin searching for the parameter values that minimize (maximize) the χ^2 (L) to sample the posterior distribution, since $P(u|D, M) \propto L$. The χ^2 for each dataset is defined as

$$\chi_{\text{data}}^2 = (d_{i,m} - d_{i,\text{data}}) C_{ij,\text{data}}^{-1} (d_{j,m} - d_{j,\text{data}}), \quad (60)$$

where d_{data} are the observable data at a certain redshift/scale factor, d_m are the model predictions at that same redshift/scale factor, and C_{data} is the covariance matrix associated with the data. If the procedure is performed for more than one model, we can compare them by using their Bayesian evidence. For two models M_1 and M_2 , we define their Bayes factor as

$$Z_{12} \equiv \frac{E(D|M_1)}{E(D|M_2)}. \quad (61)$$

The natural logarithm of this ratio can be interpreted, using a scale such as the empirical Jeffreys scale [151], to determine which model is preferred or disfavoured, and with what strength.

For completeness, we also report the reduced chi-square, defined as

$$\chi_{\text{red}}^2 \equiv \frac{\chi^2}{\nu}, \quad (62)$$

where $\nu = N_{\text{data}} - N_{\text{par}}$ denotes the number of degrees of freedom, given by the difference between the number of data points and the number of free model parameters. $\chi_{\text{red}}^2 \approx 1$ indicates a statistically acceptable fit.

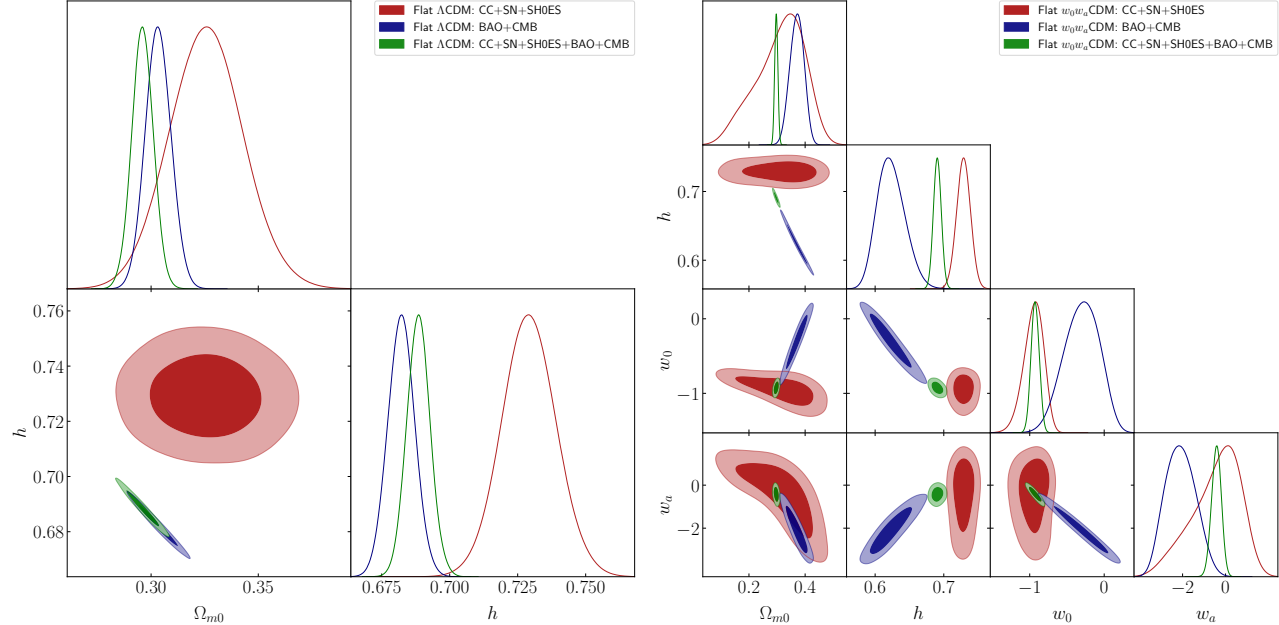
The total χ^2 , the reduced χ_{red}^2 , and the Bayesian Evidence are provided in Tables III, IV, and V. The number of data points for each datasets considered in this work are summarized here for convenience: $N_{\text{data}} = 15$ (CC), 1590 (SNe), 1 (SH0ES), 13 (BAOs), and 3 (CMB), respectively.

VI. COSMOLOGICAL RESULTS

Tables III and IV summarise the constraints on the cosmological parameters obtained from analyses based on the **CC+SN+SHOES** and **BAO+CMB** dataset combinations,

Priors										
Model	h	Ω_{m0}	w_0	w_a	w_E	α	β	ξ	γ	μ
Λ CDM	(0.4, 0.9)	(0.1, 0.5)	—	—	—	—	—	—	—	—
w_0w_a CDM	(0.4, 0.9)	(0.1, 0.5)	(-3.0, 1.0)	(-3.5, 2.0)	—	—	—	—	—	—
PC1	(0.4, 0.9)	(0.1, 0.5)	—	—	(-3.0, 1.0)	(0.0, 10.0)	(-2.0, 2.0)	—	—	—
PC2	(0.4, 0.9)	(0.1, 0.5)	—	—	—	—	—	(-1.0, 0.5)	—	—
PC3	(0.4, 0.9)	(0.1, 0.5)	—	—	(-3.0, 1.0)	—	—	—	(-3.0, 3.0)	—
PC4	(0.4, 0.9)	(0.1, 0.5)	—	—	(-3.0, 1.0)	—	—	—	(-3.0, 3.0)	(-3.0, 3.0)

TABLE II. Flat uniform priors used for each model.

FIG. 1. Triangular plots showing the 1D and 2D posterior distributions for the Λ CDM (left panels) and w_0w_a CDM (right panels) models, obtained using the CC+SN+SH0ES, BAO+CMB, and full CC+SN+SH0ES+BAO+CMB dataset combinations.

respectively. These complementary analyses are designed to explicitly investigate the Hubble tension by isolating late-time and early-time information within different cosmological models.

From the inferred values of H_0 and their corresponding 1σ uncertainties, we find that the tension between the two dataset combinations reaches the level of 4.3σ in the Λ CDM scenario and 5.2σ in the w_0w_a CDM model. Within the PC framework, the tension is partially alleviated, being reduced to 2.4σ , 3.0σ , 2.6σ , and 2.4σ for the PC1, PC2, PC3, and PC4 models, respectively. This mitigation is achieved without introducing strong departures from the standard expansion history, highlighting the ability of particle-creation mechanisms to improve consistency between late-time observations and high-redshift constraints.

However, it is worth noting that the alleviation of the H_0 tension is largely driven by the larger uncertainties on H_0 inferred from the BAO+CMB combination in the PC models, while the central values remain close to the corre-

sponding Λ CDM value. Indeed, in the BAO+CMB analysis, H_0 is relatively weakly constrained within the w_0w_a CDM and PC models. This behaviour is expected, as these scenarios are constructed to deviate from Λ CDM only at late times, making them predominantly sensitive to low-redshift observables rather than to early-Universe physics.

To maximise the constraining power and improve the overall performance of the models, we present a joint analysis combining all available datasets, CC+SN+SH0ES+BAO+CMB. The corresponding parameter constraints are reported in Table V, together with the total χ^2 values and Bayesian evidences.

From the results in Table V, we find that the PC models yield a lower minimum χ^2 than Λ CDM, with an improvement of $\Delta\chi^2_{\min} \simeq 8$ when introducing up to three additional parameters. However, the reduced chi-square remains essentially unchanged ($\chi^2_{\text{red}} = 0.894$ in Λ CDM compared to $\chi^2_{\text{red}} = 0.890$ for the PC models), and the Bayesian evidence is statistically indistinguish-

Constraints on cosmological parameters from CC+SN+SH0ES							
Model	H_0 (km s $^{-1}$ Mpc $^{-1}$)	Ω_{m0}	Extra parameters	χ^2_{\min}	χ^2_{red}	$\log Z$	
Λ CDM	72.92 ± 0.99 [72.92]	0.326 ± 0.017 [0.325]	—	1411.403	0.880	-712.45	
w_0w_a CDM	72.88 ± 0.99 [73.00]	$0.312_{-0.066}^{+0.100}$ [0.197]	$w_0 = -0.95_{-0.12}^{+0.15}$ [-0.84] $w_a = -0.42_{-0.83}^{+1.40}$ [0.63]	1411.047	0.881	-715.29	
PC1	72.94 ± 0.94 [73.04]	$0.331_{-0.047}^{+0.056}$ [0.352]	$w_E = -0.89_{-0.37}^{+0.29}$ [-1.02] $\alpha = 3.3_{-3.1}^{+1.6}$ [9.7] $\beta = 0.56_{-0.52}^{+1.00}$ [-0.92]	1411.024	0.881	-714.37	
PC2	72.92 ± 0.99 [72.89]	$0.319_{-0.045}^{+0.039}$ [0.303]	$\xi = 0.03_{-0.25}^{+0.38}$ [-0.18]	1411.168	0.880	-712.66	
PC3	72.90 ± 0.99 [72.85]	$0.309_{-0.038}^{+0.057}$ [0.240]	$w_E = -1.04_{-0.40}^{+0.50}$ [-0.35] $\gamma = 0.69_{-0.62}^{+1.10}$ [0.79]	1411.111	0.881	-714.12	
PC4	72.91 ± 0.94 [73.09]	$0.309_{-0.041}^{+0.057}$ [0.240]	$w_E = -1.00 \pm 0.47$ [-1.39] $\gamma = 0.3 \pm 1.4$ [-1.4] $\mu = 0.4_{-1.4}^{+1.7}$ [2.7]	1411.108	0.881	-714.29	

TABLE III. Mean values and 68 % confidence-level uncertainties for the cosmological parameters in the Λ CDM, w_0w_a CDM, and PC models constrained with the CC+SN+SH0ES datasets. The corresponding best-fit values are reported in square brackets when they differ from the mean values. The last three columns list the χ^2_{\min} , the reduced χ^2_{red} , and the logarithm of the Bayesian evidence (marginal likelihood) Z obtained with nested sampling.

Constraints on cosmological parameters from BAO+CMB							
Model	H_0 (km s $^{-1}$ Mpc $^{-1}$)	Ω_{m0}	Extra parameters	χ^2_{\min}	χ^2_{red}	$\log Z$	
Λ CDM	68.22 ± 0.49 [68.22]	0.303 ± 0.006 [0.303]	—	14.827	1.059	-19.98	
w_0w_a CDM	$62.3_{-2.2}^{+1.8}$ [62.5]	0.371 ± 0.025 [0.368]	$w_0 = -0.30_{-0.22}^{+0.26}$ [-0.33] $w_a = -2.10_{-0.76}^{+0.68}$ [-2.00]	5.996	0.500	-19.23	
PC1	$67.2_{-1.4}^{+2.2}$ [64.3]	$0.316_{-0.023}^{+0.014}$ [0.345]	$w_E = -1.05_{-0.56}^{+0.76}$ [-1.99] $\alpha = 1.69_{-1.60}^{+0.99}$ [0.01] $\beta = 0.77_{-0.41}^{+0.62}$ [1.46]	6.856	0.623	-20.13	
PC2	68.72 ± 1.01 [68.69]	0.300 ± 0.009 [0.300]	$\xi = 0.01 \pm 0.12$ [0.01]	11.129	0.856	-19.32	
PC3	$65.5_{-2.4}^{+2.7}$ [64.6]	$0.334_{-0.032}^{+0.024}$ [0.342]	$w_E = -1.73_{-0.50}^{+0.64}$ [-1.92] $\gamma = 1.39_{-0.27}^{+0.43}$ [1.46]	6.831	0.569	-19.01	
PC4	$65.8_{-2.3}^{+2.8}$ [64.5]	$0.331_{-0.032}^{+0.023}$ [0.344]	$w_E = -1.03 \pm 0.78$ [-1.99] $\gamma = 0.12 \pm 1.84$ [1.40] $\mu = 0.85 \pm 1.34$ [0.04]	6.806	0.619	-19.22	

TABLE IV. Same as Table III, but with parameter constraints obtained using the BAO+CMB datasets.

able among all models. According to Bayesian model comparison, this indicates that the PC scenarios are neither preferred nor disfavoured with respect to Λ CDM by current data. Nevertheless, their ability to achieve a comparable goodness of fit while allowing for a physically motivated extension of the late-time dynamics demonstrates that particle creation constitutes a viable and statistically competitive alternative to the standard cosmological model.

The marginalised posterior distributions for the flat Λ CDM and w_0w_a CDM models are shown in Fig. 1, while the corresponding triangle plots for the PC models are displayed in Fig. 2. All posterior analyses and corner

plots were produced using the `GetDist` package [152].

Figure 3 shows the evolution of the quantity $H(z)/(1+z)$ for the four PC models over the redshift range $0 < z < 3$, computed from the marginalised posterior distributions obtained using the full dataset combination. The shaded regions represent the 95% confidence intervals, obtained with the `fgivenx` package [153]. For comparison, the Λ CDM prediction corresponding to the best-fit parameters in Table V is also shown. Despite the additional degrees of freedom introduced by particle creation, all PC models closely track the Λ CDM expansion history, even at late times, reflecting the strong constraints imposed by the combined datasets.

Constraints on cosmological parameters from CC+SN+SH0ES+BAO+CMB							
Model	H_0 (km s $^{-1}$ Mpc $^{-1}$)	Ω_{m0}	Extra parameters		χ^2_{\min}	χ^2_{red}	$\log Z$
Λ CDM	68.85 ± 0.43 [68.86]	0.296 ± 0.005 [0.296]	–		1448.026	0.894	−736.62
w_0w_a CDM	69.06 ± 0.56 [69.04]	0.297 ± 0.006 [0.297]	$w_0 = -0.93 \pm 0.05$ [−0.93] $w_a = -0.43 \pm 0.22$ [−0.36]		1443.728	0.892	−740.06
PC1	69.32 ± 0.49 [69.28]	0.294 ± 0.005 [0.295]	$w_E = -0.98_{-0.17}^{+0.21}$ [−0.86] $\alpha = 2.1_{-1.8}^{+1.2}$ [2.1] $\beta = 0.62_{-0.43}^{+0.75}$ [0.85]		1439.288	0.890	−736.15
PC2	69.34 ± 0.55 [69.35]	0.293 ± 0.005 [0.293]	$\xi = -0.011 \pm 0.073$ [−0.010]		1440.975	0.890	−735.26
PC3	69.28 ± 0.50 [69.23]	0.294 ± 0.005 [0.295]	$w_E = -1.12_{-0.11}^{+0.20}$ [−1.24] $\gamma = 0.98_{-0.44}^{+0.78}$ [1.17]		1439.463	0.890	−735.63
PC4	69.28 ± 0.49 [69.27]	0.294 ± 0.005 [0.295]	$w_E = -1.02_{-0.17}^{+0.19}$ [−1.10] $\gamma = 0.26 \pm 1.46$ [2.88] $\mu = 0.63 \pm 1.26$ [−1.49]		1439.420	0.890	−735.57

TABLE V. Same as Table III, but with parameter constraints obtained using the full combination of datasets CC+SN+SH0ES+BAO+CMB.

A closer inspection of the constraints reported in Table V reveals that, for PC1, PC3, and PC4, the parameter w_E is fully consistent with the Λ CDM limit $w_E = -1$ at the 1σ level, while for PC2 the same conclusion applies to the parameter ξ , whose Λ CDM value $\xi = 0$ is also recovered within 1σ . This result further confirms that the PC models naturally converge towards Λ CDM in the region of parameter space preferred by current observations.

The requirement of an accelerating Universe is satisfied by all PC models. Using the best-fit parameters from Table V, one can explicitly verify that the theoretical acceleration conditions derived in Sect. IV are fulfilled, *i.e.*, the conditions given in Eq. (14), or equivalently Eqs. (30), (32), and (33) for the PC1, PC3, and PC4 models. For the PC2 model, instead, we evaluate the effective equation-of-state parameter of dark energy and verify that $w_{\text{DE}}^{\text{eff}}(z) < -1/3$.

Table VI reports the present-day values of the deceleration parameter q_0 for all models using the combined CC+SN+SH0ES+BAO+CMB dataset, while Fig. 4 shows its redshift evolution, $q(z)$, obtained from the functional posterior distributions. In this context, we used Eqs. (41)–(44) and (35). All scenarios exhibit a transition from decelerated to accelerated expansion at $z < 1$ and remain consistent with Λ CDM within 2σ . Moreover, both q_0 and the present-day effective dark-energy equation of state, $w_{\text{DE}}^{\text{eff}}(0)$, agree with the Λ CDM expectations at the 1σ level for all PC models.

An important outcome of our analysis concerns the physical nature of the created component. From Table V, we find that in all four PC models the additional component satisfies $w_E < -1/3$, implying behaviour compatible with dark energy in the standard cosmological scenario. This result is particularly significant, as the equation-of-state parameter w_E was treated as a completely free quantity, following an agnostic approach with

no prior assumptions on the nature of the created particles. The data therefore indicate that, even within a particle-creation framework, a dark-energy-like component is required to account for the late-time dynamics of the Universe.

In this context, Fig. 5 illustrates the redshift evolution of the fractional energy densities $\Omega_m(z)$, $\Omega_r(z)$, and $\Omega_E(z)$ (defined as usual as $\Omega_i(z) = \rho_i(z)/\rho_{\text{crit}}(z)$ for component i , with $\rho_{\text{crit}}(z) = 3H^2(z)/\chi$). The plot refers to the PC1 model, but the same qualitative behaviour applies to the other PC models. The contribution of the created component dominates the energy budget in the local Universe, while becoming rapidly negligible at high redshift compared to matter and radiation, which follow their standard scaling. This behaviour provides further evidence that the newly created particles effectively act as a dark-energy component, leaving early-Universe physics unaltered.

Conversely, scenarios corresponding to the production of pressureless matter particles ($w_E = 0$) are strongly disfavoured by the data, being excluded at the 4.7σ , 5.6σ , and 5.4σ levels for the PC1, PC3, and PC4 models, respectively. This represents a substantial departure from earlier studies, which primarily focused on the creation of cold dark matter particles, and highlights the importance of confronting particle-creation scenarios with current high-precision cosmological data. At the same time, the constraints on w_E do not allow us to distinguish conclusively between an effective quintessence-like regime and phantom behaviour, differently from [78], where the dark energy particle production is associated with the bulk viscosity..

The effective dark-energy equation of state, $w_{\text{DE}}^{\text{eff}}(z)$, is shown in Fig. 6 for all PC models and compared with the corresponding confidence regions obtained within the w_0w_a CDM framework. We use Eqs. (50)–(53) and

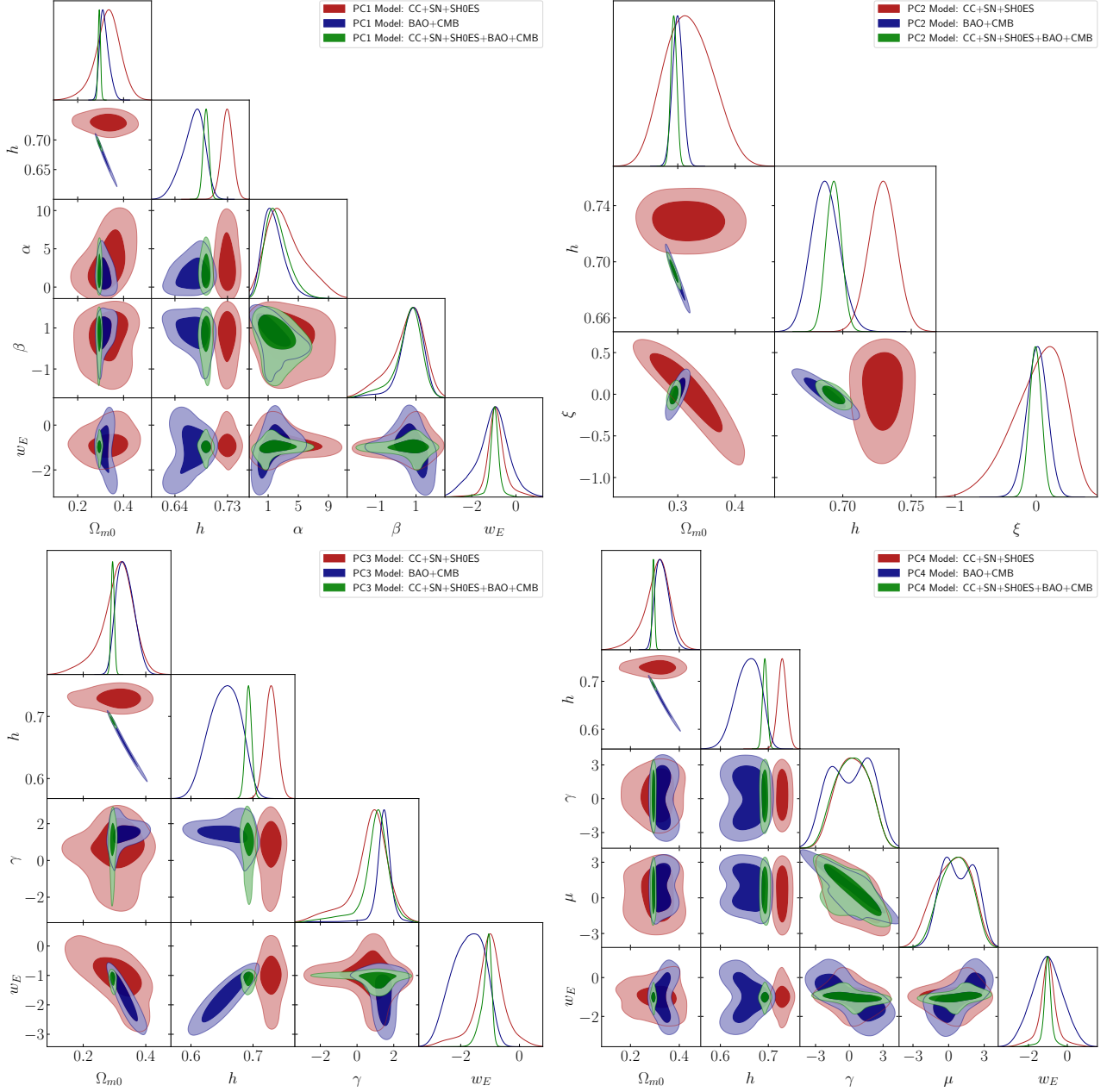


FIG. 2. Triangular plots showing the 1D and 2D posterior distributions for the PC models using the CC+SN+SH0ES, BAO+CMB, and full CC+SN+SH0ES+BAO+CMB dataset combinations. The panels correspond to PC1 (top left), PC2 (top right), PC3 (bottom left), and PC4 (bottom right).

Derived parameters for the CC+SN+SH0ES+BAO+CMB analysis						
	Λ CDM	$w_0 w_a$ CDM	PC1	PC2	PC3	PC4
q_0	-0.56 ± 0.01	-0.48 ± 0.06	-0.55 ± 0.03	-0.56 ± 0.03	$-0.54^{+0.03}_{-0.05}$	$-0.54^{+0.03}_{-0.04}$
$w_{\text{DE}}^{\text{eff}}(0)$	-1	-0.93 ± 0.05	$-0.99^{+0.02}_{-0.03}$	-1.00 ± 0.02	$-0.98^{+0.03}_{-0.04}$	$-0.99^{+0.02}_{-0.04}$

TABLE VI. Derived parameters (mean values and 68 % confidence-level uncertainties) for the flat Λ CDM, $w_0 w_a$ CDM, and PC models, obtained from the statistical distributions of cosmological parameters inferred from the CC+SN+SH0ES+BAO+CMB dataset combination (see Table V). The first row reports the deceleration parameter evaluated at the present epoch, $z = 0$ (see Eqs. (41), (42), (43), and (44)). The second row reports the effective dark-energy equation-of-state parameter evaluated at $z = 0$ (see Eqs. (50), (51), (52), and (53)).

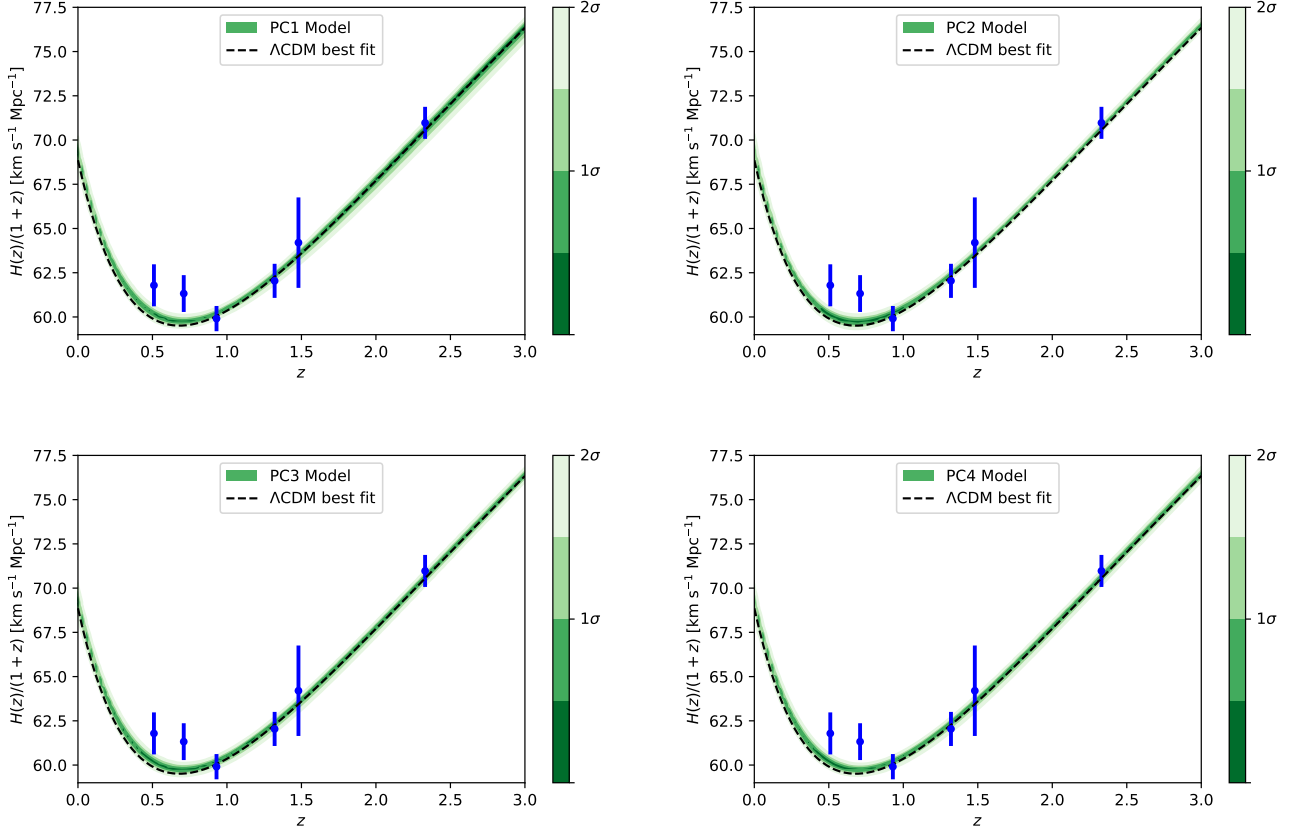


FIG. 3. Plots of the function $H(z)/(1+z)$ for the PC models. The upper panels show the PC1 (left) and PC2 (right) models, while the lower panels show the PC3 (left) and PC4 (right) models. The functional posterior distributions are shown up to the 2σ level, based on the parameter constraints reported in Table V for the CC+SN+SHOES+BAO+CMB dataset combination. For comparison, the dashed curve corresponds to the Λ CDM model, using the best-fit parameter values from Table V. The blue data points with error bars indicate the DESI DR2 BAO measurements, included as an illustrative subset of the data to demonstrate the agreement with observations.

the functional posterior distributions derived from the CC+SN+SHOES+BAO+CMB analysis. Table VI also reports the present-day values ($z = 0$) of the effective equation-of-state parameter for all PC models.

In all cases, the condition $w_{\text{DE}}^{\text{eff}}(z) < -1/3$ is satisfied, confirming the presence of accelerated expansion. The PC2 model, which is equivalent to a w CDM scenario with a constant equation of state, yields a value of $w_{\text{DE}}^{\text{eff}}$ fully consistent with a cosmological constant at the 1σ level. Similarly, the PC3 and PC4 models remain compatible with Λ CDM within 1σ across the full redshift range considered. PC3 and PC4 exhibit only a mild redshift dependence of $w_{\text{DE}}^{\text{eff}}(z)$ when compared with the dynamical dark-energy behaviour obtained in the CPL parametrization (black curves in Fig. 6).

The PC1 model stands out as particularly interesting, as it displays a more pronounced dynamical evolution of $w_{\text{DE}}^{\text{eff}}(z)$ at low redshift, indicating a possible deviation from Λ CDM while remaining fully consistent with accelerated expansion. This behaviour is also reflected in

the evolution of $H(z)/(1+z)$ and $q(z)$ shown in Figs. 3 and 4. Moreover, the PC1 model exhibits a transition from an effective quintessence regime to a phantom-like behaviour at low redshift. This feature makes PC1 a useful framework for exploring departures from Λ CDM and effective dynamical dark-energy scenarios, particularly in light of recent results from the DESI collaboration [12].

VII. CONCLUSIONS

In this work, we have investigated a class of cosmological models based on particle creation (PC), aimed at providing an effective description of late-time cosmic acceleration and exploring possible implications for the H_0 tension. By adopting an agnostic approach to the nature of the created component and confronting the models with a comprehensive set of cosmological observations, we have assessed their viability in comparison with the standard Λ CDM model and dynamical dark-energy sce-

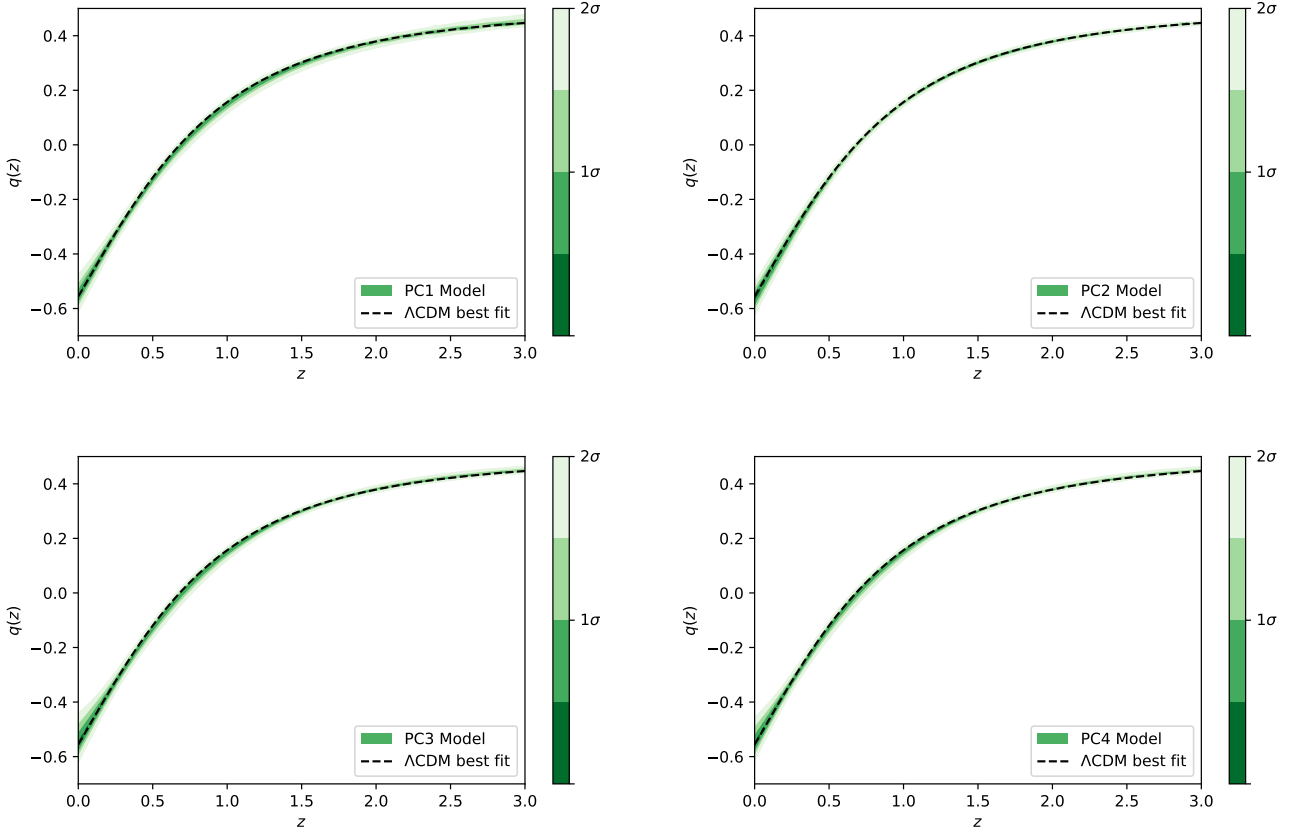


FIG. 4. Plots of the deceleration parameter $q(z)$ for the PC models. The upper panels show the PC1 (left) and PC2 (right) models, while the lower panels show the PC3 (left) and PC4 (right) models. The functional posterior distributions are shown up to the 2σ level, based on the parameter constraints reported in Table V for the CC+SN+SHOES+BAO+CMB dataset combination. For comparison, the dashed curve corresponds to the Λ CDM model, using the best-fit parameter values from Table V.

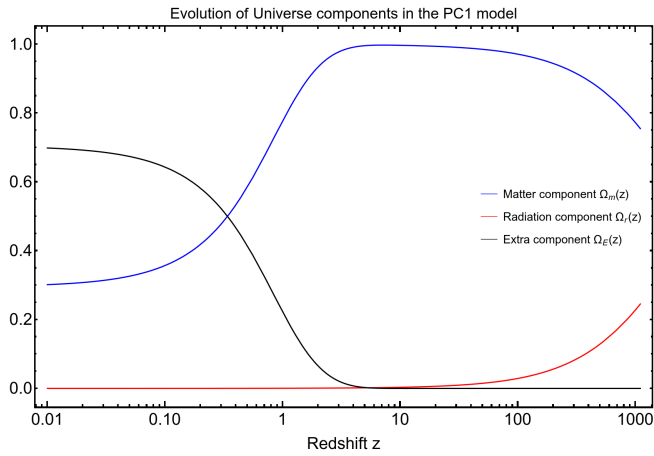


FIG. 5. Redshift evolution of the cosmological components in the PC1 model, computed using the best-fit parameter values from Table V obtained in the joint CC+SN+SHOES+BAO+CMB analysis. The fractional energy densities $\Omega_m(z)$, $\Omega_r(z)$, and $\Omega_E(z)$ are shown by the blue, red, and black curves, respectively.

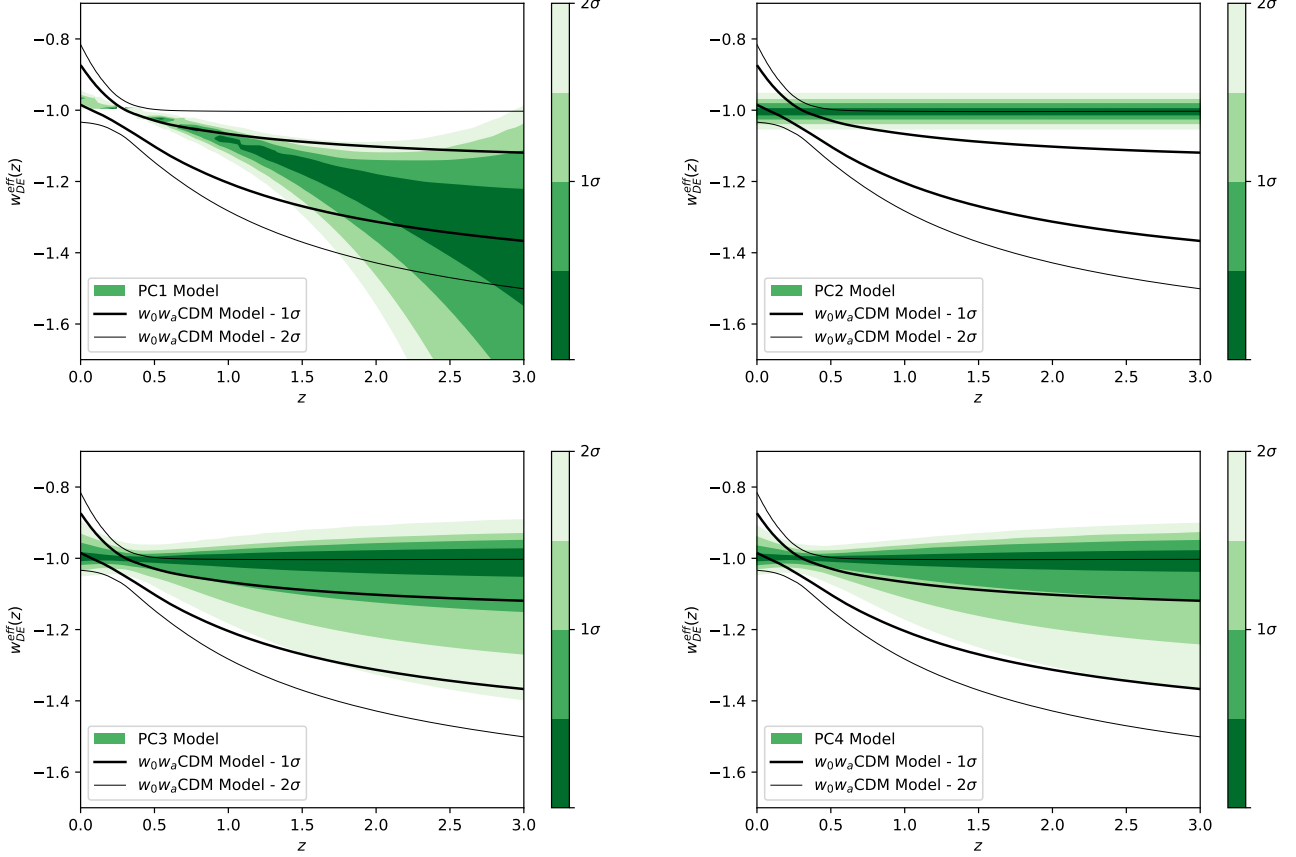


FIG. 6. Effective dark-energy equation-of-state parameter $w_{\text{DE}}^{\text{eff}}(z)$ for the PC models. The upper panels show the PC1 (left) and PC2 (right) models, while the lower panels show the PC3 (left) and PC4 (right) models. The functional posterior distributions are shown up to the 2σ level, based on the parameter constraints reported in Table V for the CC+SN+SHOES+BAO+CMB dataset combination. For comparison with a dynamical dark-energy scenario, the 1σ (black curves) and 2σ (grey curves) confidence contours associated with the $w_0w_a\text{CDM}$ model are also shown in each panel.

narios.

Using combinations of the CC, SN, SHOES, BAO, and CMB datasets, we have shown that all the PC models considered are fully consistent with current observations and provide an excellent description of the late-time expansion history of the Universe. When individual dataset combinations are analysed separately, the PC models partially alleviate the H_0 tension with respect to ΛCDM and $w_0w_a\text{CDM}$, although a residual discrepancy remains (see the discussion in Sect. VI). In the joint analysis including all datasets, the PC scenarios yield fits comparable to, and in terms of minimum χ^2 slightly better than, those of ΛCDM , while the Bayesian evidence remains statistically indistinguishable among the models (see Table V). This indicates that the PC models are neither preferred nor disfavoured with respect to ΛCDM by current data, while remaining fully consistent with early-Universe constraints.

A key outcome of our analysis is that the intrinsic equation-of-state parameter of the created component is robustly constrained by the data to satisfy $w_E < -1/3$

in all PC models, implying that the newly created particles effectively behave as a dark-energy-like component. This result is particularly significant, since the nature of the extra component was not specified *a priori* and w_E was treated as a free parameter. Our findings therefore indicate that, even within scenarios based on particle creation, a dark-energy-like component is still required by observations to explain the late-time dynamics of the Universe. Moreover, the hypothesis of particle creation in the form of pressureless matter ($w_E = 0$) at low redshift is strongly disfavoured by the data at high statistical significance, in contrast with several earlier studies that focused on cold dark matter production [23–26].

From a dynamical perspective, the PC models describe an accelerating Universe, with present-day values of the deceleration parameter and effective dark-energy equation of state fully consistent with ΛCDM within 1σ . The reconstructed evolutions of $H(z)/(1+z)$, $q(z)$, and $w_{\text{DE}}^{\text{eff}}(z)$ closely follow the ΛCDM predictions, with only mild deviations allowed at late times. In particular, all PC models exhibit a transition from deceleration to accel-

eration at $z < 1$, in agreement with standard cosmology.

An important conceptual difference with respect to phenomenological dynamical dark-energy models, such as $w_0 w_a$ CDM, lies in the redshift range over which deviations from Λ CDM are admitted. By construction, we impose $g(0) = 1$ and recover the Λ CDM expansion history at $z > 3$, in order to preserve the sound horizon at the drag epoch and allow for a consistent use of CMB data as a high-redshift BAO probe. As a consequence, departures from Λ CDM are confined to the interval $0 < z < 3$, where the continuity equation is solved numerically and particle-creation effects become relevant. This leads to a weak but non-trivial effective dynamical dark-energy behaviour, distinct from the asymptotic evolution inherent to the $w_0 w_a$ CDM model. Indeed, within the CPL parametrization one has $w(z) \rightarrow w_0$ at $z = 0$ and $w(z) \rightarrow w_0 + w_a$ asymptotically as $z \rightarrow \infty$. By contrast, our results show that the PC models remain extremely close to Λ CDM at both low and high redshift, while allowing for mild, localized deviations at intermediate redshifts.

Among the PC models explored, PC1 emerges as particularly interesting, as it allows for a more pronounced evolution of the effective dark-energy equation of state $w_{\text{DE}}^{\text{eff}}(z)$ while remaining consistent with accelerated expansion and with all background observables. This feature makes it a useful framework for exploring controlled departures from Λ CDM and for providing a physically motivated alternative to purely phenomenological dynamical dark-energy models, particularly in light of recent and forthcoming high-precision measurements from large-scale structure surveys such as DESI [12].

Finally, we note that while particle-creation models provide a consistent and physically motivated description of late-time cosmic acceleration, the parametrization of the particle-creation rate remains phenomenological. Further progress will require a deeper theoretical understanding of the underlying microphysical mechanisms, as well as an extension of the analysis to perturbations and structure formation. Moreover, allowing particle creation to operate over a broader redshift range than $0 < z < 3$ and solving the continuity equation numerically also in the early Universe may help to further develop the physical description of these models. In this work, however, we have focused on low redshifts due to numerical lim-

itations. Future observational data, in particular from next-generation galaxy surveys and improved local measurements of H_0 , will be crucial to further test this class of models and to assess their viability as alternatives to the standard cosmological paradigm.

ACKNOWLEDGMENTS

The work of TS is supported by the Della Riccia foundation grant 2025. MDA is supported by the Leverhulme Trust. EDV is supported by a Royal Society Dorothy Hodgkin Research Fellowship. This article/publication is based upon work from COST Action CA21136 Addressing observational tensions in cosmology with systematics and fundamental physics (CosmoVerse) supported by COST (European Cooperation in Science and Technology). L.A.E. acknowledges financial support from the Türkiye Bilimsel ve Teknolojik Araştırma Kurumu (TÜBİTAK, Scientific and Technological Research Council of Türkiye) through grant no. 124N627. TS and MDA acknowledge the IT Services at The University of Sheffield for providing High Performance Computing resources.

Appendix A: Preliminary analysis for choosing priors

The priors for every parameter used in the analysis presented in Sect. V are reported in Table II. They were selected after performing a preliminary study of the PC models to evaluate the impact of different values of the parameters on the Hubble function. For instance, see Figs. 7, and 8, which are referred only to the PC1 model, but the same approach was done for all our models. Equivalently, see Fig. 9 to see the impact of different values of the parameters on the effective equation of state parameter of dark energy (preliminary analysis for choosing the priors) within the PC1 model. For reference and comparison we will use the flat (zero curvature) Λ CDM model, see Fig. 1 for the marginalized posteriors of its background parameters $h \equiv \frac{H_0}{100} \text{ km}^{-1} \text{ s Mpc}$ (dimensionless Hubble constant) and Ω_{m0} using CC+BAO+SN+SHOES+CMB as the dataset combination.

[1] C. L. Bennett *et al.* (WMAP), *Astrophys. J. Suppl.* **208**, 20 (2013), [arXiv:1212.5225 \[astro-ph.CO\]](https://arxiv.org/abs/1212.5225).

[2] N. Aghanim *et al.* (Planck), *Astron. Astrophys.* **641**, A6 (2020), [Erratum: *Astron. Astrophys.* 652, C4 (2021)], [arXiv:1807.06209 \[astro-ph.CO\]](https://arxiv.org/abs/1807.06209).

[3] N. Aghanim *et al.* (Planck), *Astron. Astrophys.* **641**, A1 (2020), [arXiv:1807.06205 \[astro-ph.CO\]](https://arxiv.org/abs/1807.06205).

[4] S. Aiola *et al.* (ACT), *JCAP* **12**, 047, [arXiv:2007.07288 \[astro-ph.CO\]](https://arxiv.org/abs/2007.07288).

[5] T. Louis *et al.* (Atacama Cosmology Telescope), *JCAP* **11**, 062, [arXiv:2503.14452 \[astro-ph.CO\]](https://arxiv.org/abs/2503.14452).

[6] E. Camphuis *et al.* (SPT-3G), SPT-3G D1: CMB temperature and polarization power spectra and cosmology from 2019 and 2020 observations of the SPT-3G Main field (2025), [arXiv:2506.20707 \[astro-ph.CO\]](https://arxiv.org/abs/2506.20707).

[7] F. Beutler, C. Blake, M. Colless, D. H. Jones, L. Staveley-Smith, L. Campbell, Q. Parker, W. Saunders, and F. Watson, *Mon. Not. Roy. Astron. Soc.* **416**,

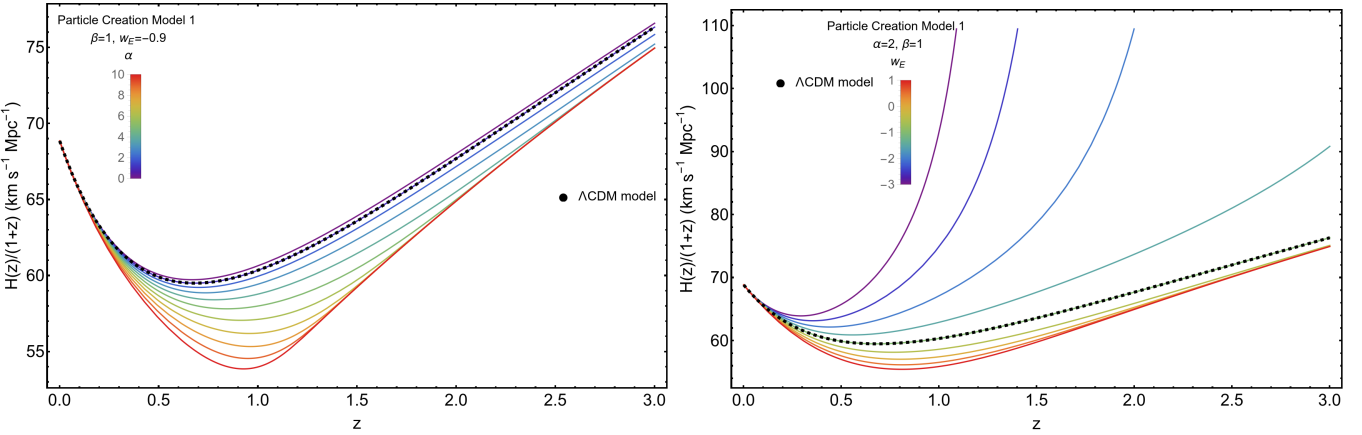


FIG. 7. Left panel: plot of the function $\frac{H(z)}{1+z}$ in the PC1 model for different values of α . The parameter w_E was fixed to the value -0.9 . The trivial case $w_E = -1$ is not interesting, since it ends up with the Λ CDM model, as it can be seen also from Eq. (19). Right panel: plot of the function $\frac{H(z)}{1+z}$ in the PC1 model for different values of w_E . The extra parameters were set $\alpha = 2$ and $\beta = 1$. For both panels, H_0, Ω_{m0} are fixed to their best-fit values within the corresponding Λ CDM model, which are reported in Table V (CC+SN+SHOES+BAO+CMB constraints). The dashed line indicates the flat Λ CDM model for a comparison.

3017 (2011), arXiv:1106.3366 [astro-ph.CO].

[8] A. J. Ross, L. Samushia, C. Howlett, W. J. Percival, A. Burden, and M. Manera, *Mon. Not. Roy. Astron. Soc.* **449**, 835 (2015), arXiv:1409.3242 [astro-ph.CO].

[9] S. Alam *et al.* (BOSS), *Mon. Not. Roy. Astron. Soc.* **470**, 2617 (2017), arXiv:1607.03155 [astro-ph.CO].

[10] S. Alam *et al.* (eBOSS), *Phys. Rev. D* **103**, 083533 (2021), arXiv:2007.08991 [astro-ph.CO].

[11] T. M. C. Abbott *et al.* (DES), *Phys. Rev. D* **105**, 023520 (2022), arXiv:2105.13549 [astro-ph.CO].

[12] M. Abdul Karim *et al.* (DESI), *Phys. Rev. D* **112**, 083515 (2025), arXiv:2503.14738 [astro-ph.CO].

[13] G. Gu *et al.* (DESI), Dynamical Dark Energy in light of the DESI DR2 Baryonic Acoustic Oscillations Measurements (2025), arXiv:2504.06118 [astro-ph.CO].

[14] A. H. Wright *et al.*, *Astron. Astrophys.* **703**, A158 (2025), arXiv:2503.19441 [astro-ph.CO].

[15] D. Brout *et al.*, *Astrophys. J.* **938**, 110 (2022), arXiv:2202.04077 [astro-ph.CO].

[16] D. Scolnic *et al.*, *Astrophys. J.* **938**, 113 (2022), arXiv:2112.03863 [astro-ph.CO].

[17] T. M. C. Abbott *et al.* (DES), *Astrophys. J. Lett.* **973**, L14 (2024), arXiv:2401.02929 [astro-ph.CO].

[18] M. Moresco, L. Pozzetti, A. Cimatti, R. Jimenez, C. Maraston, L. Verde, D. Thomas, A. Citro, R. Tojeiro, and D. Wilkinson, *JCAP* **05**, 014, arXiv:1601.01701 [astro-ph.CO].

[19] M. Moresco, Addressing the Hubble tension with cosmic chronometers (2023), arXiv:2307.09501 [astro-ph.CO].

[20] S. Weinberg, *Rev. Mod. Phys.* **61**, 1 (1989).

[21] I. Prigogine, J. Geheniau, E. Gunzig, and P. Nardone, *Gen. Rel. Grav.* **21**, 767 (1989).

[22] M. O. Calvao, J. A. S. Lima, and I. Waga, *Phys. Lett. A* **162**, 223 (1992).

[23] M. P. Freaza, R. S. de Souza, and I. Waga, *Phys. Rev. D* **66**, 103502 (2002).

[24] S. Pan, J. de Haro, A. Paliathanasis, and R. J. Slagter, *Mon. Not. Roy. Astron. Soc.* **460**, 1445 (2016), arXiv:1601.03955 [gr-qc].

[25] V. H. Cárdenas, M. Cruz, S. Lepe, S. Nojiri, and S. D. Odintsov, *Phys. Rev. D* **101**, 083530 (2020), arXiv:2004.02337 [gr-qc].

[26] E. Elizalde, M. Khurshudyan, and S. D. Odintsov, *Eur. Phys. J. C* **84**, 782 (2024), arXiv:2407.20285 [gr-qc].

[27] I. Zlatev, L.-M. Wang, and P. J. Steinhardt, *Phys. Rev. Lett.* **82**, 896 (1999), arXiv:astro-ph/9807002.

[28] J. M. d. Costa Netto and H. H. B. d. Silva, *Chin. J. Phys.* **94**, 684 (2025), arXiv:2503.00087 [gr-qc].

[29] S. R. G. Trevisani and J. A. S. Lima, *Eur. Phys. J. C* **83**, 244 (2023), arXiv:2303.01974 [astro-ph.CO].

[30] P. W. R. Lima, J. A. S. Lima, and J. F. Jesus, *Eur. Phys. J. C* **85**, 449 (2025), arXiv:2502.14139 [astro-ph.CO].

[31] H. Gohar and V. Salzano, *Eur. Phys. J. C* **81**, 338 (2021), arXiv:2008.09635 [gr-qc].

[32] R. A. C. Cipriano, T. Harko, F. S. N. Lobo, M. A. S. Pinto, and J. a. L. Rosa, *Phys. Dark Univ.* **44**, 101463 (2024), arXiv:2310.15018 [gr-qc].

[33] R. A. C. Cipriano, N. Ganiyeva, T. Harko, F. S. N. Lobo, M. A. S. Pinto, and J. a. L. Rosa, *Universe* **10**, 339 (2024), arXiv:2408.14106 [gr-qc].

[34] O. Akarsu and N. M. Uzun, *Phys. Dark Univ.* **40**, 101194 (2023), arXiv:2301.11204 [gr-qc].

[35] G. P. Singh, R. Garg, and A. Singh, *International Journal of Geometric Methods in Modern Physics* **0**, 2550111 (0), 2405.15626.

[36] M. A. S. Pinto, T. Harko, and F. S. N. Lobo, *Phys. Rev. D* **106**, 044043 (2022), arXiv:2205.12545 [gr-qc].

[37] G. Montani, N. Carlevaro, and M. De Angelis, *Entropy* **26**, 662 (2024), arXiv:2407.12409 [gr-qc].

[38] M. Marciu, *Eur. Phys. J. C* **84**, 1191 (2024), [Erratum: Eur. Phys. J. C 84, 1285 (2024)], arXiv:2410.04584 [gr-qc].

[39] S. Ganjizadeh, A. Amani, and M. A. Ramzanpour, *Chin. Phys. C* **46**, 125104 (2022), arXiv:2208.07710 [gr-qc].

[40] A. Bouali, H. Chaudhary, T. Harko, F. S. N. Lobo, T. Ouali, and M. A. S. Pinto, *Mon. Not. Roy. Astron. Soc.* **526**, 4192 (2023), arXiv:2309.15497 [gr-qc].

[41] V. H. Cárdenas, M. Cruz, and S. Lepe, *Eur. Phys. J. Plus* **139**, 642 (2024), arXiv:2302.10155 [gr-qc].

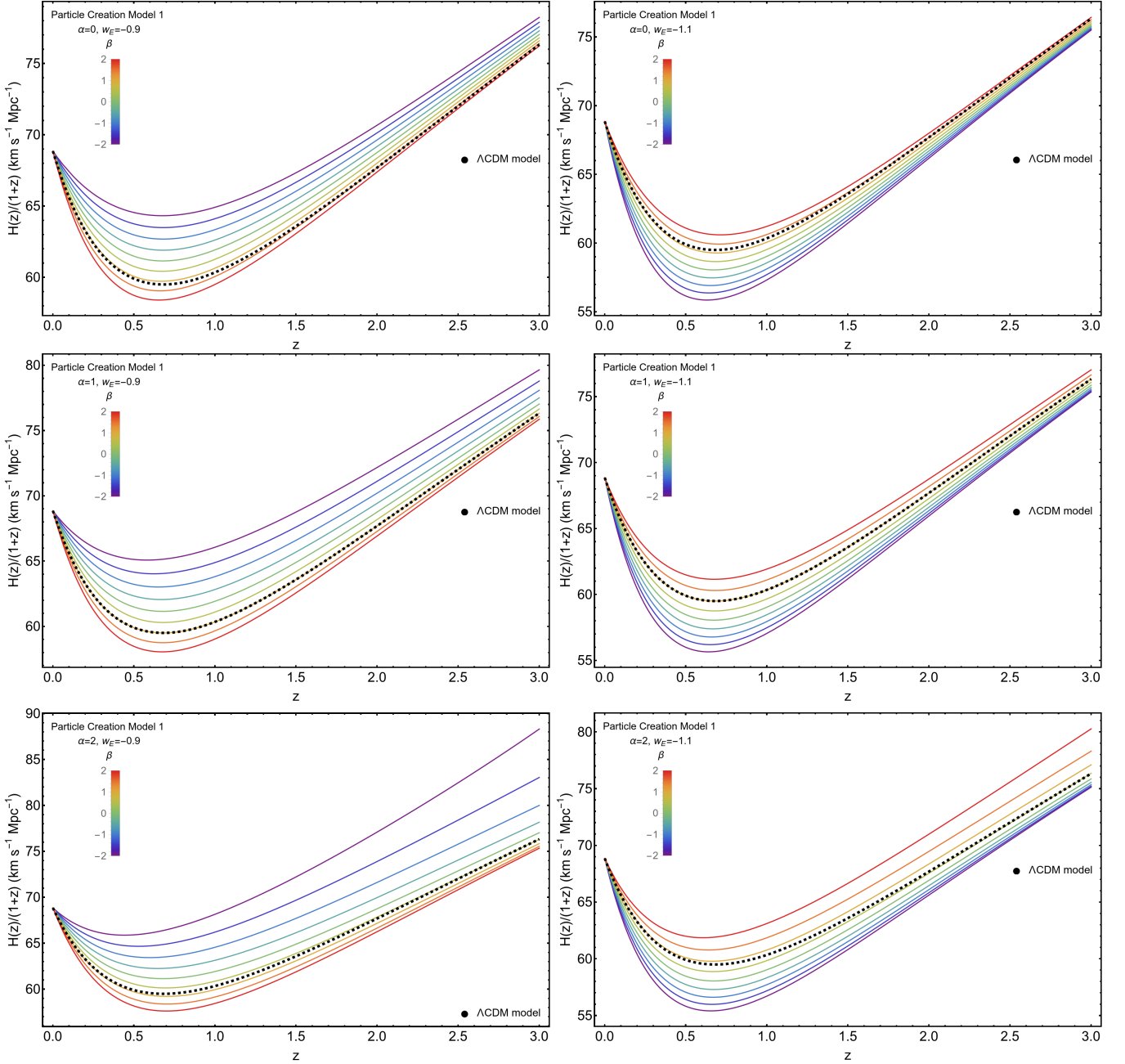


FIG. 8. Plots of the function $\frac{H(z)}{1+z}$ in the PC1 model for different values of β . The parameter w_E was fixed to the value -0.9 and -1.1 on the left and right panels, respectively. The trivial case $w_E = -1$ is not interesting, since it ends up with the Λ CDM model, as it can be seen also from Eq. (19). The upper, central, and lower panels refer to $\alpha = 0, 1, 2$, respectively. The other cosmological parameters are fixed to their best-fit values within the corresponding Λ CDM model, which are reported in Table V (CC+SN+SHOES+BAO+CMB constraints). The dashed line indicates the flat Λ CDM model for a comparison.

- [42] V. H. Cárdenas, M. Cruz, and S. Lepe, *Phys. Rev. D* **102**, 123543 (2020), arXiv:2008.12403 [gr-qc].
- [43] V. H. Cárdenas and S. Lepe, *Eur. Phys. J. C* **85**, 411 (2025), arXiv:2501.14509 [astro-ph.CO].
- [44] Y. L. Bolotin, V. A. Cherkaskiy, M. I. Konchatnyi, S. Pan, and W. Yang, *Int. J. Mod. Phys. D* **31**, 2250036 (2022), arXiv:2008.09602 [gr-qc].
- [45] L. Verde, T. Treu, and A. G. Riess, *Nature Astron.* **3**, 891 (2019), arXiv:1907.10625 [astro-ph.CO].
- [46] S. Vagnozzi, *Phys. Rev. D* **102**, 023518 (2020), arXiv:1907.07569 [astro-ph.CO].
- [47] E. Di Valentino *et al.*, *Astropart. Phys.* **131**, 102605 (2021), arXiv:2008.11284 [astro-ph.CO].
- [48] E. Di Valentino, O. Mena, S. Pan, L. Visinelli, W. Yang, A. Melchiorri, D. F. Mota, A. G. Riess, and J. Silk, *Class. Quant. Grav.* **38**, 153001 (2021), arXiv:2103.01183 [astro-ph.CO].

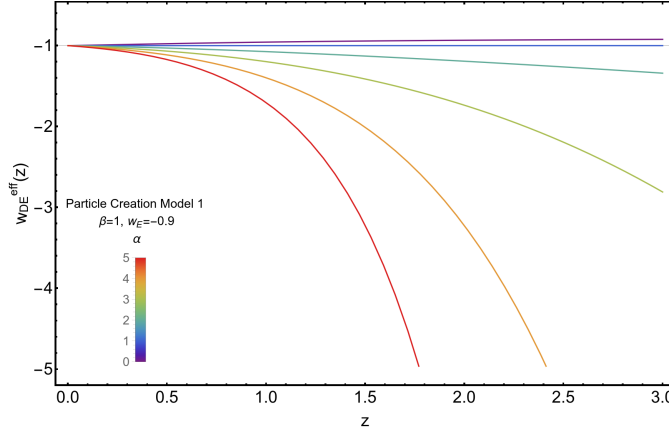


FIG. 9. Plot of the effective equation of state parameter of dark energy $w_{\text{DE}}^{\text{eff}}(z)$ in the PC1 model for different values of α . The extra parameters are set $w_E = -0.9$ and $\beta = 1$, while H_0 , Ω_{m0} are fixed to their best-fit values within the corresponding Λ CDM model, which are reported in Table V (CC+SN+SHOES+BAO+CMB constraints). The grey curve indicates the cosmological constant scenario with $w_{\text{DE}}^{\text{eff}} = -1$.

- [49] L. Perivolaropoulos and F. Skara, *New Astron. Rev.* **95**, 101659 (2022), arXiv:2105.05208 [astro-ph.CO].
- [50] N. Schöneberg, G. Franco Abellán, A. Pérez Sánchez, S. J. Witte, V. Poulin, and J. Lesgourges, *Phys. Rept.* **984**, 1 (2022), arXiv:2107.10291 [astro-ph.CO].
- [51] P. Shah, P. Lemos, and O. Lahav, *Astron. Astrophys. Rev.* **29**, 9 (2021), arXiv:2109.01161 [astro-ph.CO].
- [52] E. Abdalla *et al.*, *JHEAp* **34**, 49 (2022), arXiv:2203.06142 [astro-ph.CO].
- [53] E. Di Valentino, *Universe* **8**, 399 (2022).
- [54] M. Kamionkowski and A. G. Riess, *Ann. Rev. Nucl. Part. Sci.* **73**, 153 (2023), arXiv:2211.04492 [astro-ph.CO].
- [55] W. Giarè, *CMB Anomalies and the Hubble Tension* (2023), arXiv:2305.16919 [astro-ph.CO].
- [56] J.-P. Hu and F.-Y. Wang, *Universe* **9**, 94 (2023), arXiv:2302.05709 [astro-ph.CO].
- [57] L. Verde, N. Schöneberg, and H. Gil-Marín, *Ann. Rev. Astron. Astrophys.* **62**, 287 (2024), arXiv:2311.13305 [astro-ph.CO].
- [58] E. Di Valentino and D. Brout, eds., *The Hubble Constant Tension*, Springer Series in Astrophysics and Cosmology (Springer, 2024).
- [59] L. Perivolaropoulos, *Phys. Rev. D* **110**, 123518 (2024), arXiv:2408.11031 [astro-ph.CO].
- [60] E. Di Valentino *et al.* (CosmoVerse Network), *Phys. Dark Univ.* **49**, 101965 (2025), arXiv:2504.01669 [astro-ph.CO].
- [61] A. G. Riess *et al.*, *Astrophys. J. Lett.* **934**, L7 (2022), arXiv:2112.04510 [astro-ph.CO].
- [62] S. Casertano *et al.* (H0DN), The Local Distance Network: a community consensus report on the measurement of the Hubble constant at 1% precision (2025), arXiv:2510.23823 [astro-ph.CO].
- [63] S. D. Odintsov, D. Sáez-Chillón Gómez, and G. S. Sharov, *Nucl. Phys. B* **966**, 115377 (2021), arXiv:2011.03957 [gr-qc].
- [64] T. Schiavone, G. Montani, M. G. Dainotti, B. De Simone, E. Rinaldi, and G. Lambiase, in *17th Italian-Korean Symposium on Relativistic Astrophysics* (2022) arXiv:2205.07033 [astro-ph.CO].
- [65] T. Schiavone, G. Montani, and F. Bombacigno, *Mon. Not. Roy. Astron. Soc.* **522**, L72 (2023), arXiv:2211.16737 [gr-qc].
- [66] S. Nojiri, S. D. Odintsov, and V. K. Oikonomou, *Nucl. Phys. B* **980**, 115850 (2022), arXiv:2205.11681 [gr-qc].
- [67] G. Montani, M. De Angelis, F. Bombacigno, and N. Carlevaro, *Mon. Not. Roy. Astron. Soc.* **527**, L156 (2023), arXiv:2306.11101 [gr-qc].
- [68] L. A. Escamilla, D. Fiorucci, G. Montani, and E. Di Valentino, *Phys. Dark Univ.* **46**, 101652 (2024), arXiv:2408.04354 [astro-ph.CO].
- [69] T. Schiavone and G. Montani, *Nuovo Cim. C* **48**, 105 (2025), arXiv:2408.01410 [gr-qc].
- [70] S. D. Odintsov, D. Sáez-Chillón Gómez, and G. S. Sharov, *Eur. Phys. J. C* **85**, 298 (2025), arXiv:2412.09409 [gr-qc].
- [71] G. Montani, M. De Angelis, and M. G. Dainotti, *Phys. Dark Univ.* **49**, 101969 (2025), arXiv:2506.13288 [astro-ph.CO].
- [72] D. Efratiou, E. A. Paraskevas, and L. Perivolaropoulos, e-print (2025), arXiv:2511.04610 [astro-ph.CO].
- [73] S. D’Onofrio, S. Odintsov, and T. Schiavone, e-print (2025), arXiv:2511.06924 [gr-qc].
- [74] A. Valletta, G. Montani, M. G. Dainotti, and E. Fazzari, e-print (2025), arXiv:2512.19568 [gr-qc].
- [75] G. Montani, L. A. Escamilla, N. Carlevaro, and E. Di Valentino, *Phys. Rev. D* **113**, 023507 (2026), arXiv:2512.20193 [astro-ph.CO].
- [76] G. Montani, N. Carlevaro, and M. G. Dainotti, *Phys. Dark Univ.* **44**, 101486 (2024), arXiv:2311.04822 [gr-qc].
- [77] G. Montani, N. Carlevaro, and M. G. Dainotti, *Phys. Dark Univ.* **48**, 101847 (2025), arXiv:2411.07060 [gr-qc].
- [78] I. Navone, M. G. Dainotti, E. Fazzari, G. Montani, N. Maki, and K. Kohri, e-print (2025), arXiv:2511.16130 [astro-ph.CO].
- [79] S. Kumar and R. C. Nunes, *Phys. Rev. D* **94**, 123511 (2016), arXiv:1608.02454 [astro-ph.CO].
- [80] R. Murgia, S. Gariazzo, and N. Fornengo, *JCAP* **04**, 014, arXiv:1602.01765 [astro-ph.CO].
- [81] S. Kumar and R. C. Nunes, *Phys. Rev. D* **96**, 103511 (2017), arXiv:1702.02143 [astro-ph.CO].

[82] E. Di Valentino, A. Melchiorri, and O. Mena, *Phys. Rev. D* **96**, 043503 (2017), arXiv:1704.08342 [astro-ph.CO].

[83] S. Kumar, *Phys. Dark Univ.* **33**, 100862 (2021), arXiv:2102.12902 [astro-ph.CO].

[84] L.-Y. Gao, Z.-W. Zhao, S.-S. Xue, and X. Zhang, *JCAP* **07**, 005, arXiv:2101.10714 [astro-ph.CO].

[85] S. Pan and W. Yang, *On the interacting dark energy scenarios - the case for Hubble constant tension* (2023), arXiv:2310.07260 [astro-ph.CO].

[86] D. Benisty, S. Pan, D. Staicova, E. Di Valentino, and R. C. Nunes, *Astron. Astrophys.* **688**, A156 (2024), arXiv:2403.00056 [astro-ph.CO].

[87] W. Yang, E. Di Valentino, O. Mena, S. Pan, and R. C. Nunes, *Phys. Rev. D* **101**, 083509 (2020), arXiv:2001.10852 [astro-ph.CO].

[88] M. Forconi, W. Giarè, O. Mena, Ruchika, E. Di Valentino, A. Melchiorri, and R. C. Nunes, *JCAP* **05**, 097, arXiv:2312.11074 [astro-ph.CO].

[89] A. Pourtsidou and T. Tram, *Phys. Rev. D* **94**, 043518 (2016), arXiv:1604.04222 [astro-ph.CO].

[90] E. Di Valentino, *Mon. Not. Roy. Astron. Soc.* **502**, 2065 (2021), arXiv:2011.00246 [astro-ph.CO].

[91] E. Di Valentino and O. Mena, *Mon. Not. Roy. Astron. Soc.* **500**, L22 (2020), arXiv:2009.12620 [astro-ph.CO].

[92] R. C. Nunes and E. Di Valentino, *Phys. Rev. D* **104**, 063529 (2021), arXiv:2107.09151 [astro-ph.CO].

[93] W. Yang, A. Mukherjee, E. Di Valentino, and S. Pan, *Phys. Rev. D* **98**, 123527 (2018), arXiv:1809.06883 [astro-ph.CO].

[94] R. von Marttens, L. Lombriser, M. Kunz, V. Marra, L. Casarini, and J. Alcaniz, *Phys. Dark Univ.* **28**, 100490 (2020), arXiv:1911.02618 [astro-ph.CO].

[95] M. Lucca and D. C. Hooper, *Phys. Rev. D* **102**, 123502 (2020), arXiv:2002.06127 [astro-ph.CO].

[96] L.-Y. Gao, S.-S. Xue, and X. Zhang, *Chin. Phys. C* **48**, 051001 (2024), arXiv:2212.13146 [astro-ph.CO].

[97] Y. Zhai, W. Giarè, C. van de Bruck, E. Di Valentino, O. Mena, and R. C. Nunes, *JCAP* **07**, 032, arXiv:2303.08201 [astro-ph.CO].

[98] A. Bernui, E. Di Valentino, W. Giarè, S. Kumar, and R. C. Nunes, *Phys. Rev. D* **107**, 103531 (2023), arXiv:2301.06097 [astro-ph.CO].

[99] G. A. Hoerning, R. G. Landim, L. O. Ponte, R. P. Rolim, F. B. Abdalla, and E. Abdalla, *Phys. Rev. D* **112**, 023523 (2025), arXiv:2308.05807 [astro-ph.CO].

[100] W. Giarè, Y. Zhai, S. Pan, E. Di Valentino, R. C. Nunes, and C. van de Bruck, *Phys. Rev. D* **110**, 063527 (2024), arXiv:2404.02110 [astro-ph.CO].

[101] L. A. Escamilla, O. Akarsu, E. Di Valentino, and J. A. Vazquez, *JCAP* **11**, 051, arXiv:2305.16290 [astro-ph.CO].

[102] M. A. van der Westhuizen and A. Abebe, *JCAP* **01**, 048, arXiv:2302.11949 [gr-qc].

[103] E. Silva, U. Zúñiga-Bolaño, R. C. Nunes, and E. Di Valentino, *Eur. Phys. J. C* **84**, 1104 (2024), arXiv:2403.19590 [astro-ph.CO].

[104] E. Di Valentino, A. Melchiorri, O. Mena, and S. Vagnozzi, *Phys. Dark Univ.* **30**, 100666 (2020), arXiv:1908.04281 [astro-ph.CO].

[105] T.-N. Li, P.-J. Wu, G.-H. Du, S.-J. Jin, H.-L. Li, J.-F. Zhang, and X. Zhang, *Astrophys. J.* **976**, 1 (2024), arXiv:2407.14934 [astro-ph.CO].

[106] N. N. Pooya, *Phys. Rev. D* **110**, 043510 (2024), arXiv:2407.03766 [astro-ph.CO].

[107] S. Halder, J. de Haro, T. Saha, and S. Pan, *Phys. Rev. D* **109**, 083522 (2024), arXiv:2403.01397 [gr-qc].

[108] S. Castello, M. Mancarella, N. Grimm, D. Sobral-Blanco, I. Tutusaus, and C. Bonvin, *JCAP* **05**, 003, arXiv:2311.14425 [astro-ph.CO].

[109] Y.-H. Yao and X.-H. Meng, *Phys. Dark Univ.* **39**, 101165 (2023).

[110] K. R. Mishra, S. K. J. Pacif, R. Kumar, and K. Bamba, *Phys. Dark Univ.* **40**, 101211 (2023), arXiv:2301.08743 [gr-qc].

[111] R. C. Nunes, S. Pan, and E. N. Saridakis, *Phys. Rev. D* **94**, 023508 (2016), arXiv:1605.01712 [astro-ph.CO].

[112] E. Silva, M. A. Sabogal, M. Scherer, R. C. Nunes, E. Di Valentino, and S. Kumar, *Phys. Rev. D* **111**, 123511 (2025), arXiv:2503.23225 [astro-ph.CO].

[113] W. Yang, S. Zhang, O. Mena, S. Pan, and E. Di Valentino, e-print (2025), arXiv:2508.19109 [astro-ph.CO].

[114] M. van der Westhuizen, A. Abebe, and E. Di Valentino, *Phys. Dark Univ.* **50**, 102121 (2025), arXiv:2509.04496 [gr-qc].

[115] G. Montani, N. Carlevaro, L. A. Escamilla, and E. Di Valentino, *Phys. Dark Univ.* **48**, 101848 (2025), arXiv:2404.15977 [gr-qc].

[116] M. G. Dainotti, G. Bargiacchi, M. Bogdan, A. L. Lenart, K. Iwasaki, S. Capozziello, B. Zhang, and N. Fraija, *Astrophys. J.* **951**, 63 (2023), arXiv:2305.10030 [astro-ph.CO].

[117] M. G. Dainotti, G. Bargiacchi, M. Bogdan, S. Capozziello, and S. Nagataki, arXiv (2023), arXiv:2303.06974 [astro-ph.CO].

[118] M. G. Dainotti, G. Bargiacchi, M. Bogdan, S. Capozziello, and S. Nagataki, *JHEAp* **41**, 30 (2024).

[119] G. Bargiacchi, M. G. Dainotti, S. Nagataki, and S. Capozziello, *Mon. Not. Roy. Astron. Soc.* **521**, 3909 (2023), arXiv:2303.07076 [astro-ph.CO].

[120] M. G. Dainotti, A. L. Lenart, M. G. Yengejeh, S. Chakraborty, N. Fraija, E. Di Valentino, and G. Montani, *Phys. Dark Univ.* **44**, 101428 (2024), arXiv:2401.12847 [astro-ph.HE].

[121] K. C. Wong *et al.* (H0LiCOW), *Mon. Not. Roy. Astron. Soc.* **498**, 1420 (2020), arXiv:1907.04869 [astro-ph.CO].

[122] L. Kazantzidis and L. Perivolaropoulos, *Phys. Rev. D* **102**, 023520 (2020), arXiv:2004.02155 [astro-ph.CO].

[123] C. Krishnan, E. Ó. Colgáin, Ruchika, A. A. Sen, M. M. Sheikh-Jabbari, and T. Yang, *Phys. Rev. D* **102**, 103525 (2020), arXiv:2002.06044 [astro-ph.CO].

[124] M. G. Dainotti, B. De Simone, T. Schiavone, G. Montani, E. Rinaldi, and G. Lambiase, *ApJ* **912**, 150 (2021), arXiv:2103.02117 [astro-ph.CO].

[125] M. G. Dainotti, B. De Simone, T. Schiavone, G. Montani, E. Rinaldi, G. Lambiase, M. Bogdan, and S. Ugale, *Galaxies* **10**, 24 (2022), arXiv:2201.09848 [astro-ph.CO].

[126] E. Ó. Colgáin, M. M. Sheikh-Jabbari, and R. Solomon, *Phys. Dark Univ.* **40**, 101216 (2023), arXiv:2211.02129 [astro-ph.CO].

[127] M. Dainotti, B. De Simone, G. Montani, T. Schiavone, and G. Lambiase, *PoS CORFU2022*, 235 (2023), arXiv:2301.10572 [astro-ph.CO].

[128] X. D. Jia, J. P. Hu, and F. Y. Wang, *Astron. Astrophys.* **674**, A45 (2023), arXiv:2212.00238 [astro-ph.CO].

[129] M. Malekjani, R. M. Conville, E. Ó. Colgáin, S. Pouro-jaghi, and M. M. Sheikh-Jabbari, *Eur. Phys. J. C* **84**, 317 (2024), arXiv:2301.12725 [astro-ph.CO].

[130] E. Ó. Colgáin, M. M. Sheikh-Jabbari, R. Solomon, M. G. Dainotti, and D. Stojkovic, *Phys. Dark Univ.* **44**, 101464 (2024), arXiv:2206.11447 [astro-ph.CO].

[131] Y. Liu, H. Yu, and P. Wu, *Phys. Rev. D* **110**, L021304 (2024), arXiv:2406.02956 [astro-ph.CO].

[132] B. De Simone, M. H. P. M. van Putten, M. G. Dainotti, and G. Lambiase, *JHEAp* **45**, 290 (2025), arXiv:2411.05744 [astro-ph.CO].

[133] M. G. Dainotti *et al.*, *JHEAp* **48**, 100405 (2025), arXiv:2501.11772 [astro-ph.CO].

[134] Y.-Y. Wang, Y.-J. Li, and Y.-Z. Fan, e-print (2025), arXiv:2510.14390 [astro-ph.CO].

[135] X. D. Jia, J. P. Hu, S. X. Yi, and F. Y. Wang, *Astrophys. J. Lett.* **979**, L34 (2025), arXiv:2406.02019 [astro-ph.CO].

[136] X. D. Jia, J. P. Hu, D. H. Gao, S. X. Yi, and F. Y. Wang, *Astrophys. J. Lett.* **994**, L22 (2025), arXiv:2509.17454 [astro-ph.CO].

[137] S. Kalita, A. Uniyal, T. Bulik, and Y. Mizuno, *Astrophys. J.* **996**, 50 (2026), arXiv:2506.14947 [astro-ph.CO].

[138] M. Chevallier and D. Polarski, *Int. J. Mod. Phys. D* **10**, 213 (2001), arXiv:gr-qc/0009008.

[139] E. V. Linder, *Phys. Rev. Lett.* **90**, 091301 (2003), arXiv:astro-ph/0208512.

[140] E. Fazzari, M. G. Dainotti, G. Montani, and A. Melchiorri, *JHEAp* **49**, 100459 (2026), arXiv:2506.04162 [astro-ph.CO].

[141] G. Montani, E. Fazzari, N. Carlevaro, and M. G. Dainotti, *Entropy* **27**, 895 (2025), arXiv:2507.14048 [astro-ph.CO].

[142] J. A. S. Lima, M. O. Calvao, and I. Waga, e-print (2007), arXiv:0708.3397 [astro-ph].

[143] S. Weinberg, *Cosmology* (Oxford University Press, Oxford, UK, 2008).

[144] A. Slosar and J. A. Vazquez, <https://github.com/ja-vazquez/SimpleMC> (2020).

[145] J. Skilling, in *Bayesian Inference and Maximum Entropy Methods in Science and Engineering: 24th International Workshop on Bayesian Inference and Maximum Entropy Methods in Science and Engineering*, American Institute of Physics Conference Series, Vol. 735, edited by R. Fischer, R. Preuss, and U. V. Toussaint (AIP, 2004) pp. 395–405.

[146] J. S. Speagle, *Mon. Not. Roy. Astron. Soc.* **493**, 3132 (2020), arXiv:1904.02180 [astro-ph.IM].

[147] M. Moresco, R. Jimenez, L. Verde, A. Cimatti, and L. Pozzetti, *Astrophys. J.* **898**, 82 (2020), arXiv:2003.07362 [astro-ph.GA].

[148] K. Lodha *et al.* (DESI), *Phys. Rev. D* **112**, 083511 (2025), arXiv:2503.14743 [astro-ph.CO].

[149] U. Andrade *et al.* (DESI), *Phys. Rev. D* **112**, 083512 (2025), arXiv:2503.14742 [astro-ph.CO].

[150] N. Aghanim *et al.* (Planck), *Astron. Astrophys.* **607**, A95 (2017), arXiv:1608.02487 [astro-ph.CO].

[151] R. Trotta, *Contemp. Phys.* **49**, 71 (2008), arXiv:0803.4089 [astro-ph].

[152] A. Lewis, *JCAP* **08**, 025, arXiv:1910.13970 [astro-ph.IM].

[153] W. Handley, *The Journal of Open Source Software* **3**, 10.21105/joss.00849 (2018).